KERNFORSCHUNGSANLAGE JÜLICH GmbH
Institut für Plasmaphysik
Association EURATOM-KFA

PROPERTIES OF "DETACHED"-PLASMAS

by
U. Samm, H.Bay, P. Bogen, H. Hartwig
E. Hintz, K. Höthker, Y.T. Lie
A. Pospieszczyk, G. Ross, D. Rusbüldt
B. Schweer

Jül-2123
März 1987
ISSN 0366-0885

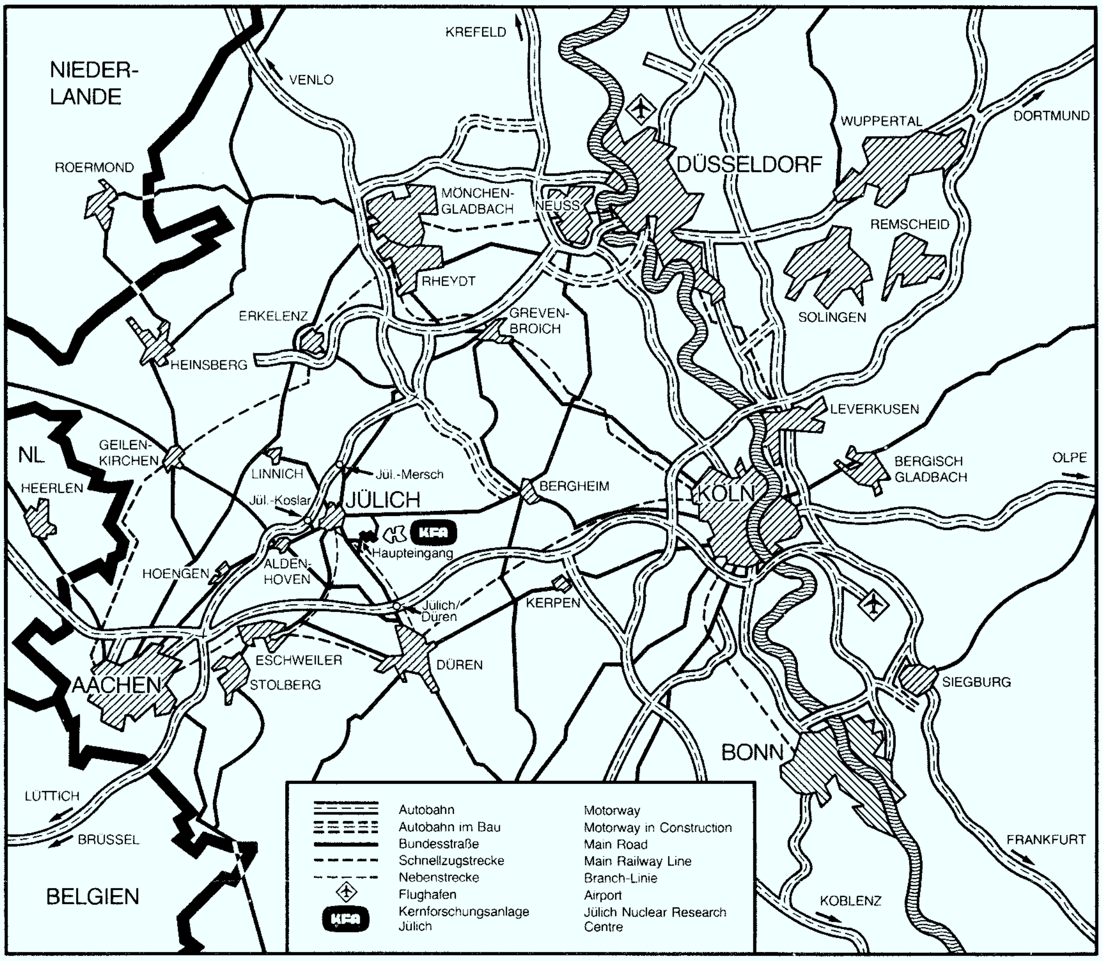

Berichte der Kernforschungsanlage Jülich – Nr. 2123

Institut für Plasmaphysik

Association EURATOM-KFA-2123

Zu beziehen durch: ZENTRALBIBLIOTHEK der Kernforschungsanlage Jülich GmbH
Postfach 1913 · D-5170 Jülich (Bundesrepublik Deutschland)
Telefon: 02461/610 · Telex: 833556-0 kf d

PROPERTIES OF "DETACHED"-PLASMAS

U. Samm, H. Bay, P. Bogen, H. Hartwig, E. Hintz, K. Höthker, Y.T.Lie ,
A. Pospieszczyk, G. Ross[1], D. Rusbüldt, B. Schweer

Institut für Plasmaphysik, KFA Jülich GmbH
Ass. EURATOM-KFA, D-5170 Jülich, FRG

---

[1]on leave from INRS-Energie, Université du Québec, Varennes, Canada

Abstract

The phenomenon "detached"-plasma is described and analyzed, based on detailed experimental studies in the TEXTOR tokamak, in particular by applying comprehensive edge diagnostics. The major parameters responsible for the transition to a "detached"-plasma are identified (heating power, electron density, impurity level) and can be related to a power loss via "100% radiation cooling" from low-Z impurities at the edge. The relevance for plasma-wall interaction, as evidenced e.g. by drastic changes in heat loads to the limiter, increase of particle flux to the wall, thereby enhancing the impurity release, is discussed. The great importance of considering the "detached"-plasma properties in scaling studies and additional heating effects is demonstrated by the impact of this plasma state on particle and energy confinement times and by ICRF-heating induced transitions.

Content

1. Introduction

The phenomenon of a "detached" plasma has first been described in[1][2] followed by more experimental evidence in [3][4][5][6] in limiter tokamaks. The phenomenon has been reviewed recently by Lipschultz [7] pointing out the relation between "detached" plasmas and MARFE's.

Generally, it has been found that the onset to this plasma state is closely correlated with the density limit [8], whereby the radiated power, mainly emitted from the boundary region, rises close to the total input power. As a major consequence the plasma is thermally disconnected from the limiter. This is linked with a shrinking of the radiative boundary layer towards smaller radii as demonstrated in Fig. 1. From the latter observation the expression "detachment from the limiter" was inferred [1]. The location of pronounced ionization of recycled neutrals being released from the limiter is also shifted inwards. This is connected with a drop of electron-temperatures and -densities at the edge, causing an increase of the penetration depth for neutrals. A summary of phenomena measured in TEXTOR is given in chapter 3.

It is argued whether thermal stability is sustained during such a change of edge radiation [8][9][10]. Both, disruptive and stable discharges in the radiation limit have been observed. But due to the large uncertainties in the parameters- theoretical and experimental - which determine the stability criteria (e.g. impurity transport, radiation function, heat conduction, impurity generation) no reliable predictions about stability could be found so far. It is generally agreed that the dominance of low-Z impurities like carbon and oxygen is in favor for stable discharges. Furthermore, operation at high q (low I_p) easier leads to stable "detached" plasmas, what can be understood if disruptions are related to the occurrence of the radiating layer close to the q=2 surface.

Most experiments and models predict that the critical density n_{ec} for the onset of a "detached" plasma is proportional to the plasma current I_p, almost parallel to the density limit (except at high I_p) [7][8][10]. Furthermore, high impurity levels decrease n_{ec}. The dependence on these parameters is discussed in chapter 4.

This type of discharges might be of great interest for fusion machines, because the extremely high radiation level from the edge leads to a plasma with a "cool, radiative plasma mantle" associated with a homogeneous distribution of power losses to the wall. But impurities are necessary to achieve a radiatively cooled plasma. Therefore the question arises what impurity concentrations are sufficient to generate a "detached" plasma and what level is acceptable for fusion machines [9] ? For the understanding of impurity generation it is of great importance to know about changes of edge parameters and particle fluxes to limiter and wall [11]. This paper deals with extensive measurements on TEXTOR related to this topic (chapter 5). In particular, the comprehensive equipment of boundary diagnostics on TEXTOR provides new insight into effects on edge-profiles, particle transport and impurity generation.

For the investigation of scaling laws - primarily the scaling with n_e - the consideration of the "detached"-plasma state can be of great importance. This will be shown in chapter 6 from the study of particle and energy confinement with "detached" plasmas and the impact of additional heating with ICRF on transitions to a "detached" plasma or vice versa.

2. Experiment

TEXTOR is a tokamak with a major radius of 1.75 m and a minor radius of typically r=46 cm. The latter is defined by a limiter system consisting of three movable, poloidal limiters, covering about 30% of the minor circumference, a movable pumplimiter (not used in this work) and two movable rail type test-limiters. There is excellent viewing access to the test-limiters, which therefore can be used for special measurements, in particular they can be withdrawn on wall level (liner at r=52-55cm) in order to provide a comparison between limiter and wall effects. The normal limiter position is r=46 cm, but it can be varied between 48 and 40 cm. It is important to note, that additional devices like a bumper limiter at the inner side of the torus at r=48.8 cm and an antenna protection limiter, poloidally closed, at r= 48.8 cm have to be considered for particle recycling at the edge.

All main limiters, the bumper limiter and the antenna protection limiter are made of graphite. Only the test limiters and the liner are metallic (stainless steel, INCONEL). But also these metal parts, facing the plasma, are normally covered by about 300 monolayers of carbon during a "carbonization" procedure [12], which is based on a glow discharge in a mixture of $CH_4(CD_4)$ and $H_2(D_2)$. Thus, TEXTOR represents under these conditions an "all-carbon" machine.

Discharges in TEXTOR can be produced with a maximum plasma current of 500 kA and a maximum toroidal magnetic field of 2.6 tesla. For the most often used conditions, 340 kA, 2 tesla, the flat top time of the plasma current is about 1 s.

The diagnostics for observing the plasma boundary are mainly based on optical methods [13]. A common feature of most of these diagnostics is the spectroscopical observation of neutral particles penetrating into the plasma boundary. Active injection of atom beams as well as the recycled neutrals at limiter and wall are used. Two methods for injecting neutral particles are applied:

1. A thermal lithium beam is generated with an oven at 800K [14]. The penetration depth is $n_e \cdot l \approx 2 \cdot 10^{12} cm^{-2}$. For electron temperatures above 10 eV the measurement of the radial emission profiles of LiI allows to deduce the electron density profiles $n_e(r)$.

2. An atom beam with 5-15 eV energy is produced by ablating thin films from a glass plate with a Ruby-laser. The penetration length is about $1 \cdot 10^{13} cm^{-2}$, thus allowing to measure some cm inside the plasma. By using lithium the n_e-profiles can be determined [15]. A combination of lithium and carbon and the comparison of the two different emission profiles allows to deduce also $T_e(r)$ at the boundary [16].

The intrinsic neutral particle beams produced by the recycling process at limiter and wall are used to determine the particle fluxes itself and to get information about plasma density and temperature at the edge. The total number of photons is quite a good measure for the total number of ionizations [17]. Although the ratio of ionizations/photon depends rather strongly on T_e, the corrections for varying T_e-profiles is rather small (20-30%). This is due to the compensating effect of increasing penetration depth of neutral particles with decreasing edge temperature. Mainly when T_e and n_e drop simultaneously then the ionizations occur nearly at constant T_e. Thus integral measurements of excitation lines like H_α, CI or OI provide rather reliable information about particle fluxes. The light was spectroscopically resolved by grating spectrometers and interference filters. As detectors were used photo-multipliers, Si-diodes and CCD-cameras.

The heat flux to the limiters is measured by infrared thermography using a peltier cooled PbSe detector with scanning optics or a CCD-camera. The latter one is less useful for the type of discharges discussed herein, because the level of convective heat fluxes to the limiters is too low to produce surface temperatures which are within the sensitive range of this detector.

3. Formation and characterization of the "detached"-plasma state

The transition of a plasma into a "detached" state is accompanied by characteristic changes of some plasma parameters. In Fig. 2a the time traces of the H_α intensities from limiter and wall and of the electron densities in the center and near the edge are shown. At the beginning of the discharge, in the "non-detached" phase, the central density as well as the edge density and the H_α-radiation at the limiter increase. Beyond a critical central density $\bar{n}_{ec}$ the edge density (r>40cm) and the H_α-radiation from the limiter start to decrease, whereas the H_α-radiation from the wall-region increases. The latter observation indicates an enhancement of the recycling flux at the wall. Therefore, the expression "detached"-plasma can be misleading. In fact, the reason for the displacement of the radiative zone is a strong reduction of electron-temperature T_e and -density n_e at the boundary, which causes the neutral particles being released from wall and limiter to increase their penetration depth and hence to shift the belt in which excitation and ionization processes become pronounced.

The same variation of parameters is observed when comparing stationary conditions with a density scan, wherein from shot to shot the density in the flat top phase of the discharge is increased. One of these discharges is displayed in Fig. 2b. The corresponding central density is $\bar{n}_e$=$3.3{\cdot}10^{13}cm^{-3}$ leading to a stationary "detached" plasma for the whole flat top time of more than 1 s. The density scan data are summarized for a variety of signals in Figs. 3a-j and will be discussed in the following.

The decrease of T_e and n_e at the edge is a consequence of the strong increase of the power loss via radiation, which reduces the convective power loss to the limiter to nearly negligible values. We define the power loss sharing between radiation (which may include charge exchange neutrals) and convective losses to the limiters by

$$\alpha = P_{rad}/P_{heat}$$

$$1-\alpha = P_{conv}/P_{heat} \quad ,$$

or

$$P_{conv} = (1/\alpha - 1)P_{rad} \quad . \qquad (1)$$

Normally, TEXTOR is operating with a rather high fraction of radiative losses α=0.7-0.8. Thus, a fairly small relative increase of radiation (e.g.25%) causes a drastic reduction of the convective losses (factor 5), as has been measured for the transition to the "detached"-plasma state. From the relation $Q \propto n_e T_e^{3/2}$ between the heat flux Q to the limiter and n_e, T_e at the limiter edge it follows that at least one of these edge parameters must decrease.

The typical decrease of T_e, n_e and Q for a transition to a "detached"-plasma is shown in Fig. 4. This drop of both parameters by nearly a factor of two has been determined by edge diagnostics which are based on the spectroscopic observation of injected atom beams. Fig. 5. shows n_e-profiles from a density scan measured with a thermal Li-beam during the flat top phase of the discharge. Below a critical central density of $\bar{n}_{ec}(0)=3.1\cdot10^{13}cm^{-3}$ the edge density rises with $\bar{n}_e(0)$. Above this critical density the n_e-profiles drop to much smaller values and a significant flattening near the limiter edge occurs. These measurements have been performed close to the main-limiter (toroidal distance 75 cm) and therefore represent a relevant parameter for the flux to the limiter.

A different diagnostic, which injects simultaneously Li and C atoms with 10-15 eV by the use of laser ablation, allows to deduce the n_e- and T_e-profiles further inside the plasma. The profiles measured at a toroidal position, which is far away from the limiter (>5m), are shown in Fig. 6 for a similar density scan as in Fig. 5. The same drop of edge density and flattening of profiles near the limiter radius takes place for the "detached"-plasma case, whereas near the wall, the drop of n_e, as observed close to the limiter, is not present. This difference will be important for further discussions on particle flux sharing between limiter and wall (see chapter 5.1). The T_e values at the limiter edge during the "attached-detached"-plasma transition drop by about a factor of 2. The 4 cm inward displacement of the radiative zone of the "detached"-plasma coincides rather well with the shoulder-like flat region of the n_e-profile and the reduced T_e-profile, where ionization and excitation processes nearly vanish. These results obtained from neutral beam spectroscopy are confirmed by measurements of

$\bar{n}_e$(r=40cm) with a HCN-interferometer [18] and by the determination of T_e(r=45.5cm) by using Thomson scattering [19] as shown in Figs. 3d,f.

The critical density $\bar{n}_{ec}$ differs between the two density scans shown in Figs. 5 and 6 because the measurements have been made during two days when the conditions (plasma current and impurities) of the machine were different. This is discussed in chapter 4.

The pronounced reduction of n_e and T_e at the edge occurring with a transition to a "detached"-plasma is connected with the strong decrease of heat flux to the limiters, as has been measured by infrared thermography. This measurement proves that in the "detached"-plasma state, nearly all power losses are going via radiation (including a small contribution from charge exchange neutrals). An illustrative example for the evolution towards such a "100%-radiation-level" is given by Boody for a TFTR discharge [6] in which the transition to a "detached"-plasma starts in an asymmetric state (Fig. 7). At the inner side of the plasma enhanced radiation is observed by bolometry. This toroidally symmetric but poloidally asymmetric phenomenon has been named "MARFE" [7]. The MARFE shown in Fig. 7 is rotating slowly while the radiation is still increasing. After some 100 ms the radiation zone becomes poloidally symmetric and located at a minor radius significantly smaller than before - the plasma settles in the "detached"-state.

In TEXTOR MARFE's are normally suppressed, due to the application of a feedback system for the horizontal plasma-position control, which makes use of the n_e-profile measurements obtained by HCN-interferometry [20]. This system is, of course, sensitive to asymmetric density variations, which develop e.g. in connection with a MARFE. Because the enhanced radiation zone of a MARFE is correlated with particle influx from the wall, a shift of the plasma column such that less plasma-wall contact occurs near to the MARFE, will diminish the asymmetry. Therefore, in TEXTOR it is possible to obtain directly a stationary, reproducible, "detached"-plasma state without the transient MARFE (see Fig. 2b). Hence we will concentrate in the following on the stationary "detached"-plasma and omit the MARFE's.

At the presence of such high radiation levels one may argue about the thermal stability of the discharge. Theoretical models [9][10] have shown that the radiation from light impurities, like carbon, from the outer zones of the plasma seems to be in favor for preventing the thermal collapse. In TEXTOR, carbon and oxygen are the dominant impurities since the walls are normally carbonized and the limiters are made of graphite. Metal impurities can be neglected. This change-over to an "all-carbon machine" increased significantly the density limit accompanied by the frequent occurrence of long lasting, stable "detached"-plasmas within the expanded density range. Before carbonization, in an "all-metal" machine, "detached"-plasmas were rarely seen in TEXTOR and normally lead to major disruptions.

4. The major parameters for the transition to a "detached"-plasma

Based on the fact that a "detached"-plasma develops only when the total radiated power P_{rad} comes close to the heating power, the most relevant parameters are obviously I_p, $\bar{n}_e$ and the density of impurities n_i. By assuming that approximately $P_{rad} \propto \bar{n}_e\, n_i$, it is possible to characterize the threshold behavior. When a discharge evolves and $\bar{n}_e$ rises, the radiation increases with

$$P_{rad} = C\, \bar{n}_e^2\, f_i \qquad (2)$$

where f_i is the relative impurity level $f_i = n_i/\bar{n}_e$ and C is a constant representing the radiation function for the impurity species under consideration. The critical density n_{ec} is reached when $P_{rad} \approx P_{heat}$. Thus we get the condition for detachment

$$\bar{n}_{ec} = (P_{heat}/Cf_i)^{1/2} \quad . \qquad (3)$$

There are two possibilities to increase $\bar{n}_{ec}$: either P_{heat} increases or f_i decreases. For both cases the experimental evidence is discussed in the next chapters.

4.1 Heating power

Fig. 8a shows the result of measurements obtained from a series of discharges with different plasma currents (i.e. different P_{heat}) and rising density during the discharge until a major disruption occurs. Two limiting curves can be derived: the critical-density curve which divides this parameter space into the "detached"- and the "non-detached"-zone and the density-limit. As expected, $\bar{n}_{ec}$

rises when going to higher currents. Moreover the relation $P_{rad} \propto \bar{n}_{ec}^2$ is found to be quite well fulfilled as is expected for a constant f_i during the density rise (Fig. 8b).

It should be noted that the margin between n_{ec} and the density-limit becomes smaller at higher currents as is seen in Fig. 8a. This fact is plausible if one considers the density limit to be reached when the radiating layer shrinks up to the q=2 surface.

Of course, there are deviations from the relation between P_{rad}, $\bar{n}_e$ and n_i as can be expected in view of the crude simplifications which have been made. The most important phenomena which induce such deviations are 1) profile effects which may cause a non-proportionality between $\bar{n}_e$ and the density in the radiating layer and 2) a density dependent impurity level $f_i(\bar{n}_e)$. For example, $\bar{n}_{ec}$ can vary within 30% for discharges with a steep $\bar{n}_e$-ramp compared to a density scan with stationary $\bar{n}_e$ (Fig. 9). But the general behavior characterized by rising $\bar{n}_{ec}$ with increasing P_{heat} is always fulfilled.

4.2 Impurity level

It has been observed that discharges with constant parameters (I_p, $\bar{n}_e$) may change over from a "detached" into a "non-detached" state only by applying 10 min of glow-discharge cleaning between the shots. Also a fresh carbonization, after which a minimum of impurities is found in the discharges, shifts $\bar{n}_{ec}$ to higher values. Then the margin between $\bar{n}_{ec}$ and the density limit can nearly vanish. Quantitative measurements of the carbon flux and of the deuterium flux being released from the main limiter during the flat top phase of the discharge have been made for a density scan under two different impurity conditions (Fig. 10). The inversion of the deuterium flux behavior, indicating the critical density $\bar{n}_{ec}$, shows up in both cases. But the value for $\bar{n}_{ec}$ is significantly lower in case 1, for which, as expected, the carbon flux is clearly higher than in case 2 for the same $\bar{n}_e$. This observation confirms qualitatively the relation (3). In addition, there is an indication of a threshold-like level of impurity influx which may be derived from the fact that the critical density in both cases is reached when the carbon flux exceeds the same value of about 3.4% of the deuterium flux.

The ratio of carbon/deuterium-flux in the "detached"-phase as a function of $\bar{n}_e$ is shown in Fig. 11, exhibiting a strong increase from 3% up to about 7%. Even considering that these values have to be somewhat corrected for the T_e-dependence, this is a very drastic jump of relative impurity fluxes, the reason of which is discussed in chapter 5.2. A major consequence of this rise of relative impurity flux (see also Fig. 3h-i) is an increase of the carbon content in the plasma core as is measured by soft-x-ray diagnostics [21] shown in Fig. 3j. The concentration of C rises from about 1.5% to 2.5%. In these measurements the light impurities C and O have been distinguished by assuming a ratio of 1:1 for C:O in the center similar to the observed flux ratio of C and O at the limiter [22]. This change of fluxes results in an increase of Z_{eff} from 2. to 3.2 associated with a rise of the loop voltage by about 25% (Fig. 3g).

The total amount of radiated power from these low-Z impurities can be estimated by assuming a radiating layer of constant thickness, impurity concentration and electron-density. The density of radiated power from C and O according to reference [10] is about 10^{-25} W/(cm$^3 n_e n_i$) for each species. Taking a density of $\bar{n}_e=0.8\cdot10^{13}$cm^{-3} and impurity concentrations of 2% each, then the radiation density is about 0.26 W/cm^3. Assuming a layer thickness of 4 cm the total radiated power amounts to 325 kW and agrees indeed with the condition $P_{rad}=P_{heat}$ (340 kA, U_p=0.9 V).

4.3 Scaling and stability

Several attempts have been made to determine experimentally and predict theoretically a scaling for the onset of MARFE's or a "detached plasma" [7][8][10]. According to reference [7], the characteristic parameter is given by

$$\rho = \frac{\bar{n}_e}{I_p/\pi a^2} \qquad \left[\frac{10^{20}\mathrm{m}^{-3}}{\mathrm{MA/m}^2} \right]$$

In most machines this parameter is ρ=0.4-0.7. A scaling of n_{ec} with $\bar{n}_e$ in ALCATOR for the occurrence of MARFE's [7] gave ρ=0.55±0.05. The corresponding value derived from TEXTOR measurements vary between 0.48 and 0.67. The major disadvantage of this scaling is the missing of impurity parameters. A comparison of ρ for the density scans in Fig. 10 shows that ρ varies between 0.49 to 0.56 only due to the different impurity levels. The models of Neuhauser [10] and Wesson [8] include the impurity concentration $f_i=n_i/n_e$. The first paper [10] predicts a relation $n_{ec}\propto f_i^{-1/2}$ (compare with eq.3), whereas the second one formulates a correlation between n_{ec} and the density limit $n_{ec}/n_{el} \propto f_i^{-1/2}$. Both scalings are qualitatively confirmed by our measurements.

But there are significant changes of parameters measured on TEXTOR - in particular the impurity behavior and the change of Z_{eff} - which are not well recognized in scaling and stability models so far. We may refine the relation (2) for the radiated power

$$P_{rad} = C\, n_{er}\, n_{ir}\, a_r\, \Delta_r \qquad (4)$$

by introducing the local electron- and impurity-densities n_{er} and n_{ir} within the radiative layer which is located at the minor radius a_r having the thickness Δ_r. An increase of radiation leads to a drop of T_e at the edge what causes an inward shift of the radiative layer - assuming that the radiation occurs at about constant T_e. Furthermore, the penetration depth of neutrals being released from wall and limiter increases, thus moving also the ionization zone inwards what results in a decrease of n_e at the edge. The continuing contraction of the plasma leading to thermal collapse due to this behavior can be prevented by the following mechanisms which act expansively:

a) The radiating volume is reduced with a shrinking a_r and with Δ_r assumed not to rise, as can be expected from the steepening of the profiles.

b) The electron density n_{er} may change much less than $\bar{n}_e$. This can only be confirmed by improving the knowledge about the location of the radiating layer and by considering the measured n_e-profiles (see Fig. 6).

c) A significant enhancement of P_{heat} due to the increase in U_p counterbalances the radiation. The reasons for this increase of U_p can be

- increase of impurity sources (see chapter 5.2)
- increase of particle confinement τ_p for impurities (see chapter 6.1)
  (on the other hand, a rise of impurity density acts contractively)
- increase of plasma resistance due to the shrinking of the current channel

Of all parameters discussed above and measured in TEXTOR (see Fig. 3), f_i and

U_p show the strongest increase with $\bar{n}_e$ during detachment. The consideration of this behavior may be important for modelling of plasmas at the radiation limit.

5. Interaction of "detached"-plasmas with the wall-limiter-system

The heat load distribution in a detached plasma is ideal. But what are the disadvantages and what problems arise with this special type of discharge? Mainly the strong increase of the impurity level has to be analyzed in more detail. In the next chapters the particle fluxes with "detached" plasmas and their correlation with impurity generation processes is discussed.

5.1 Particle flux sharing between limiter and wall

The design of a limiter is based on the idea that this device should serve as a sink for all the charged particle flux to the plasma boundary. In an extremely (hypothetical) "detached"-plasma, in which the toroidal plasma flow at the edge vanishes completely due to the edge cooling, the special wall-structures like limiters, pump-limiters or open divertors don't play anymore a role - radial particle diffusion dominates. In such a case the particle flux will be distributed uniformly over all parts of the wall. However, such an extreme case ($T_e(a)=0$) has never been observed in TEXTOR. Even for the strongest "detached"-plasmas the fraction of total particle flux taken by the limiter is still about 20%.

A better understanding of particle transport at the boundary can be found with the analysis of the 2-dimensional structure of the scrape-off-layer (SOL). As reported in a previous paper [23], measurements of n_e-profiles in the SOL of TEXTOR at different toroidal coordinates with respect to the limiters have shown that the variation of the e-folding length λ_n of n_e is significant. Close to the limiter (0.75m) the profiles are almost constant and much steeper compared to locations far away from the limiter (Fig. 12a). A numerical 2-dimensional model calculation for the SOL [24], based on electron-ion fluid equations and assuming ambipolarity can explain this behavior by taking into account additional particle sources from recycled neutrals in the vicinity of the limiter. The calculated, characteristic flow velocity being directed towards the limiter in a flux tube inside the SOL is shown in Fig. 12b. Far away from the limiter, the velocity is rising linearly whereas close to the limiter the velocity increases progressively. The n_e-profile for the major part of the flux tube, which shows the linear behavior, is given by $\lambda_n = \sqrt{DL/0.3c_s}$ where D is the cross-field diffusion coefficient, L is the length of the flux tube (connection length/2) and c_s is the ion sound speed $c_s = \sqrt{(T_e+T_i)/m_i}$. This profile determines the flux of particles to the wall : with increasing λ_n more particles will hit the wall if the distance between wall and limiter is of the order of λ_n, what is the case in TEXTOR. Assuming D and L to be constant we get the relation $\lambda_n \propto c_s^{-1/2}$. In contrast, the particle flux to the limiter is given by $\Gamma_H = n_e' \, c_s \, \lambda_n'$. Because $\lambda_n' \neq \lambda_n$ and $\lambda_n' \approx$const the dependence of the flux to the limiter on c_s is opposite to the behavior of the fluxes to the wall $\Gamma_H \propto c_s$. The decrease of the electron density close to the limiter ($n_e' < n_e$) makes this effect even stronger (see Fig. 12b). From this different dependence on c_s we can conclude that cooling of the boundary plasma leads to the following behavior: the flux to the limiter decreases, the flux to the wall increases.

This general behavior of particle flux sharing is demonstrated in Fig. 13 in which the measured deuterium fluxes (H_α) to limiter and wall are shown for different plasma currents but constant central density. The highest fluxes to the limiter and the lowest fluxes to the wall occur, as expected, with the highest current (maximum heating power). Less heating changes the flux sharing between limiter and wall in favor for the wall. An example for a "detached"-plasma showing a minimum of flux to the limiter is also indicated in Fig. 13.

This unavoidable increase of particle flux to the wall, when strong edge cooling is present, has important influence on the generation of impurities.

5.2 Generation of impurities

It is generally agreed that there are two major processes for impurity generation in tokamaks: 1) physical sputtering by ions impinging on the limiter and wall [25] and 2) chemical erosion [26][22]. In a "detached"-plasma the energy of the ions and furthermore the sheath potential at the limiter surface is lowered so much, that physical sputtering can be reduced to a negligible level. In contrast, chemical erosion is not sensitive to this variation of ion energy, but will mainly vary with the particle flux. Thus, from an increase of particle flux to the wall an enhancement of impurity production via chemical reactions at the wall surface can be expected. Indeed, this has been observed as is shown in Figs. 10 and 11. In a transition to the "detached"-plasma state the deuterium flux at the limiter decreases but the carbon flux released from the limiter still increases slightly. This observation cannot be explained with the deuterium flux to the limiter. There are probably two main processes which provide this carbon release at the limiter.

1) The enhanced particle fluxes to the wall generate a rising oxygen release from the wall. The oxygen is ionized inside the SOL and is then partly transported to the limiter (see Fig. 3h) where it can erode carbon atoms via the formation of CO with nearly 100% efficiency [27].

2) The production of hydro-carbon molecules on wall and limiter is strongly enhanced during the "detached"-plasma phase - for which the reason is yet unknown to us. Experimental evidence comes from the spectroscopic observation of molecular lines which exhibit an increase (Fig. 14) and from the measurements of doppler-shift broadening of H_α-lines [28] which indicated the existence of pronounced CH_4 dissociation at the limiters.

We conclude that the transition to a "detached"-plasma state in a tokamak with carbon-wall/limiter shifts the impurity generation processes from physical sputtering towards chemical erosion according to which the impurity level in the plasma can be sustained or even increased.

The question whether the lack of enhanced chemical erosion, as it may occur in machines with wall/limiter materials other than carbon, can hinder the transition to a stationary "detached"-plasma has to be analyzed. It seems to be difficult to sustain the pure radiatively cooled plasma if impurity generation would only go via physical sputtering.

6. Impact of "detached"-plasmas on confinement and ICRH

The change of general properties of a discharge in a "detached"-plasma state has to be considered for the study of scaling laws - in particular n_e-scaling. The enhancement of the impurity level has to be clarified, which may indicate a change in particle transport properties. Furthermore, the τ_E-scaling with $\bar{n}_e$ is affected by the occurrence of "detached" plasmas.

6.1 Particle confinement

The determination of the global particle confinement time according to the standard procedure is, even for relative measurements, very difficult. It is necessary to know the total number of particles in the discharge and the sum of all particle sources, obtained from H_α-measurements at limiters and wall. During the transition to the "detached"-plasma the fluxes at limiter and wall change inverse to each other. Therefore, the calibration and weight factors for the different H_α-measurements have a sensitive influence on the determination of the change of total influx of particles. Fig. 15 shows the global particle confinement time for a density scan. Above the critical density τ_p is enhanced by nearly a factor of 2. In view of the large uncertainties mentioned above, this observation allone cannot be a proof for a change in particle transport. But further support comes from other observation.

Another approach to determine the particle confinement time is based on the assumption that the total flux of particles losses may be calculated from the measured n_e-profiles instead of taking the influx of particles from H_α-measurements. Assuming a cross-field diffusion coefficient D=const, a particle flux Γ_H driven by a density gradient dn_e/dr at the edge of the SOL (r=46 cm) $\Gamma_H = D \; O \; dn_e/dr$, where O is the total boundary surface, the particle confinement time is obtained $\tau_P = N_{tot}/\Gamma_H$. The measured gradients evaluated from Fig. 6a and the corresponding τ_P values, calculated with D=5000 cm^2/s [29] are shown in Fig. 16. According to this method τ_P increases by about a factor of 2 in the "detached"-plasma state. Of course, it is possible to reverse the arguments by assuming that τ_P scales with n_e. Then it follows that D is increasing by a factor of 2 in the "detached"-plasma state.

An increase of confinement for impurities is more clearly demonstrated. Iron atoms have been injected by laser ablation into a "detached" and a "non-detached"-plasma [30]. The time traces of the intensities of the FeXXI, FeXX and FeXIX lines which radiate from the plasma center are shown in Fig. 17. In the "non-detached" case the iron lines die out with a time constant of about 100 ms whereas in the "detached" case the decay time is longer than 1 s (longer than the flat top of the plasma current). It is evident from this observation that the local particle confinement time for Fe is enhanced by more than a factor of 10.

Also the intrinsic impurities like carbon show an enhanced confinement as can be derived from the carbon flux and the carbon concentration shown in Figs. 3h and j. τ_p increases by about a factor of 2 in the "detached" plasma phase.

6.2 Energy confinement

The energy confinement time τ_E [31] normally is proportional to n_e (for low $\bar{n}_e$), as is shown in Fig. 3g for a density scan and in Fig. 18 for a discharge with rising density. In the latter case τ_E is in the "detached" state about 25% lower than before. This degradation of τ_E may be explained by a reduction of the effective plasma radius - defined by the location of the radiative layer - , according to the neo-Alcator scaling $\tau_E \propto n_e\ a\ q^\alpha$, where a is the plasma radius and q the safety factor and α=0.5-1. If we take α=1 and consider that $q(a) \propto a^2$ then we find $\tau_E \propto a^3$. A reduction of the effective plasma radius of about 4 cm (r=46→42 cm, Fig. 1) then indeed, results in a 25% reduction of τ_E.

The decrease of τ_E with a "detached"-plasma can be the main reason for saturation effects of τ_E at high densities as it is observed in many machines. Because the critical density for "detachment" depends on several parameters, discharges can evolve which are at the same n_e "detached" or "non-detached". Therefore, it is of great importance to know in which state a plasma is when comparing different situations. In particular this is essential for the analysis of incremental confinement times with additional heating as has been pointed out by Weynants [32].

6.3 ICRH

Additional heating by radio frequency waves at the ion-cyclotron resonance (ICRH), as applied in TEXTOR [33], may play a passive or an active role for the transition to a "detached"-plasma. If the plasma becomes "detached" then the maximum power of RF to be coupled to the plasma is limited. Generally, the switch on of ICRH changes two of the most important parameters which determine the threshold for the transition to detachment : P_{heat} and n_e. The balance between increase of heating power and density decides whether the plasma changes from "detached" to "non-detached" or vice versa or remains as it is. All these transitions have been observed in TEXTOR [32] and some examples are presented in the following.

In Fig. 19 the radial H_α-profiles at the upper main limiter of two discharges are compared. Both discharges have similar parameters (I_p, $\bar{n}_e$) and a constant power of 400 kW ICRH during the time 0.8-1.5 s. Inbetween these two discharges a glow discharge cleaning procedure lasting for about 20 min has been performed, thereby reducing mainly the oxygen contamination of the wall. This reduction of the impurity level causes a drastic change of the plasma response to the switch-on of ICRH. In the first discharge the plasma becomes "detached" (reduced H_α-intensity, long penetration depth for H/D). The corresponding surface temperature T_L on the main limiter is shown in Fig. 20. With constant heatflux Q it is expected that T_L rises proportional to $\sqrt{t}$. It is evident from Fig. 20 that the additional heating power is fully radiated away in the "detached" plasma case; the heat flux is the same for the ohmic and the RF phase of the discharge. In the second discharge the plasma remains "non-detached". The heat flux to the limiter is enhanced by about a factor of 2.5 compared to the ohmic case. This shows that, under consideration of the increase of heating power of about a factor of 2, the power sharing ratio α is somewhat reduced. Normally ICRH experiments have been performed after a fresh carbonization in order to prevent "detached" plasmas and to assure a minimum of impurities and maximum of coupled power.

An example for a discharge which is "detached" during the ohmic phase and which becomes "non-detached" with the switch-on of ICRH is given in Fig. 21a. In order to clarify the different effects, the evolution of the discharge in time in the $\bar{n}_e$-P_{heat} diagram is shown schematically in Fig. 21b. When the RF is switched on (point A), the increase of heating power overcompensates the increase of density, such that the plasma changes to a "non-detached" state. It is possible to have a discharge under slightly different conditions which remains "non-detached" in the ohmic phase and in which the application of RF (point B) leads to about the same final parameters as in the first example. In order to analyze the heating efficiencies and the incremental energy confinement times a comparison of τ_E between the ohmic and the ICRH phase of the discharge have to be made. It is evident from Fig. 21b that the comparison with point A ("detached", low τ_E) or with point B ("non-detached", high τ_E) gives different incremental τ_E. A detailed discussion of this phenomenon is given in reference [32].

7. Summary and conclusions

All important phenomena occurring with a "detached"-plasma, can be related to radiation cooling" via low-Z impurities near the edge approaching 100% of the total power losses. The dominating parameters which determine the threshold for developing a "detached"-plasma are heating power, average electron density and impurity density. Strong edge cooling reduces T_e and therefore the toroidal plasma flow to the limiters and enhances particle fluxes to the wall. This fact demonstrates the strongly diminishing relevance of limiters or other edge-devices in the "detached"-plasma case. The impurity release from the wall, due to the enhanced particle fluxes to the wall, the increase of τ_p, and the existence of notable chemical erosion (CO, CH_x) in a machine with carbon wall/limiter, assure a high radiation level during the "detached"-plasma phase. Impurity contamination in the plasma center can be enhanced to a Z_{eff} of more than 3. The enhancement of ohmic heating which is correlated with the Z_{eff} increase may be an important mechanism to stabilize the "detached" plasma. Indications for reduced particle transport, i.e. increase of τ_P for H, C and Fe, have been found. A significant deterioration of τ_E is evident during a "detached"-plasma. This reduction is consistent with a decrease of the effective minor radius according to neo-Alcator scaling.

The possibility of generating stationary tokamak discharges with a cool radiative plasma mantle, at the presence of 3-5% C and O at the edge and 1.5-2.5% C and O (each) in the center, has been shown. The impurity level is still marginal for running a fusion machine. Further detailed investigations are needed to show if the impurity screening can be improved such that this type of discharge is useful for a reactor.

Acknowledgement

The excellent experimental conditions provided by the TEXTOR team are gratefully acknowledged. For the use of supplementary data we wish to thank the following experimental physicists: A.Castracane (Fe-injection), E.Graffmann (Thomson scattering), G.Fuchs (diamagnetic loops), L.Könen (Spectrometer), J.Schlüter (soft-x-rays), H.Soltwisch (HCN interferometer) and G.Waidmann (loop voltage). The authors would like to thank R.Weynants for fruitful discussions about energy confinement with ICRH. Great support came from theoretical calculations and discussions by H.Gerhauser and H.A.Claassen.

References

[1] J.D. Strachan et.al., Proceedings of 12th Europ. Conf. on Plasma Physics and Controlled Fusion, Budapest 1985, Vol. 1, p 339

[2] J. O^Rourke et.al., Proceedings of the 12th Europ. Conf. on Plasma Physics and Controlled Fusion, Budapest 1985, Vol. 1, p. 155

[3] U. Samm et.al., Proceedings of the 11th Symposium on Plasma Engineering, Austin TX, 1985, IEEE CH2251-7, Vol.1, p.66

[4] G.M. McCracken et. al., Journal of Nucl. Mat. 145-147 (1987), p.181

[5] J.D. Strachan et. al., Journal of Nucl. Mat., Vols. 145-147, p.181

[6] F.P. Boody et. al., Journal of Nucl. Mat., Vols.145-147, p.196

[7] B. Lipschultz, Journal of Nucl. Mat., Vols.145-147, p.15

[8] J. Wesson et. al., Proceedings of the 12th Europ. Conf. on Plasma Physics and Controlled Fusion, (EPS, Geneva), Vol.1, p.339, 1985

[9] D.E.T.F. Ashby and M.H. Hughes, J. of. Nucl. Mat., 111&112 (1982)454

[10] J. Neuhauser, W. Schneider, R. Wunderlich, Report IPP 5/8, Garching FRG, 1985

[11] R.E. Waltz, K.H. Burrell, Nucl. Fusion 17 (1977) 1001

[12] J. Winter, Journal of Nucl. Mat., Vols.145-147, p.131

[13] E. Hintz, P. Bogen, in "Physics of Plasma-Wall Interactions in Controlled Fusion", Plenum Press, New York, 1986, Eds. D.E. Post and R. Behrisch

[14] Y.T. Lie et. al., Proceedings of the Int. Conf. on Plasma Physics, Lausanne 1984, vol.2, p.320

[15] A. Pospieszczyk and G.G. Ross, submitted to Rev. of Sci. Instr.

[16] A. Pospieszczyk and G.G. Ross, Proceedings of the 14th Europ. Conf. on Controlled Fusion and Plasma Physics, Madrid 1987

[17] P. Bogen et.al., J. Nucl. Mater., 128 (1984) 157

[18] H. Soltwisch, Proceedings of IEA Kyoto, 1986

[19] E. Graffmann, private communication

[20] H. Soltwisch, Nucl. Fus. Vol.23, no.12, p.1681, 1983

[21] J. Schlüter, private communication

[22] A. Pospieszczyk et al., Journal of Nucl. Mat., Vols.145-147, p.574

[23] U. Samm et al., Journal of Nucl. Mat., Vols.145-147, p.206

[24] H. Gerhauser and H.A. Claassen, Proceedings of the 12th Europ. Conf. on Plasma Physics and Controlled Fusion, Budapest 1985, Vol.2, p.464

[25] K. Behringer, Journal of Nucl. Mat., Vols.145-147, p.145

[26] J. Roth, Journal of Nucl. Mat. 145-147 (1987) p.87

[27] E. Vietzke et. al., Journal of Nucl. Mat., Vols.145-147, p.425

[28] P. Bogen et. al., to be published

[29] F. Wagner, Nucl. Fusion, 25, (1985) 525

[30] A. Castracane, to be published

[31] G. Fuchs et. al., Proceedings of the 13th Europ. Conf. on Controlled Fusion and Plasma Heating, Schliersee 1986

[32] R.R. Weynants et. al., to be published

[33] A.M. Messiaen et. al., Proceedings of the 12th Europ. Conf. on Plasma Physics and Controlled Fusion, Budapest 1985

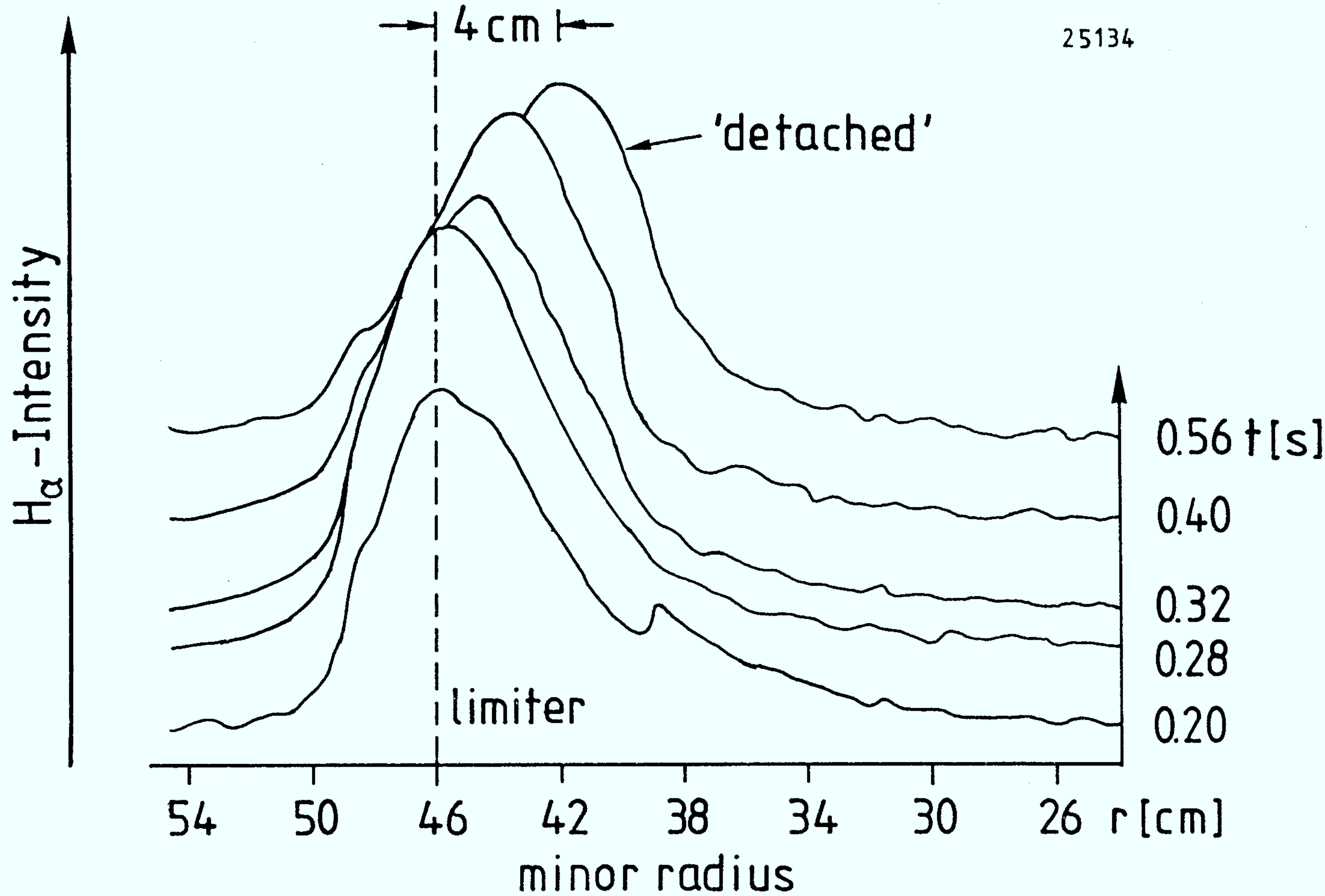

Fig. 1 3-dimensional presentation of radial H_α-profiles at the upper main limiter as a function of time. The electron-density rises leading to a "detached"-plasma.

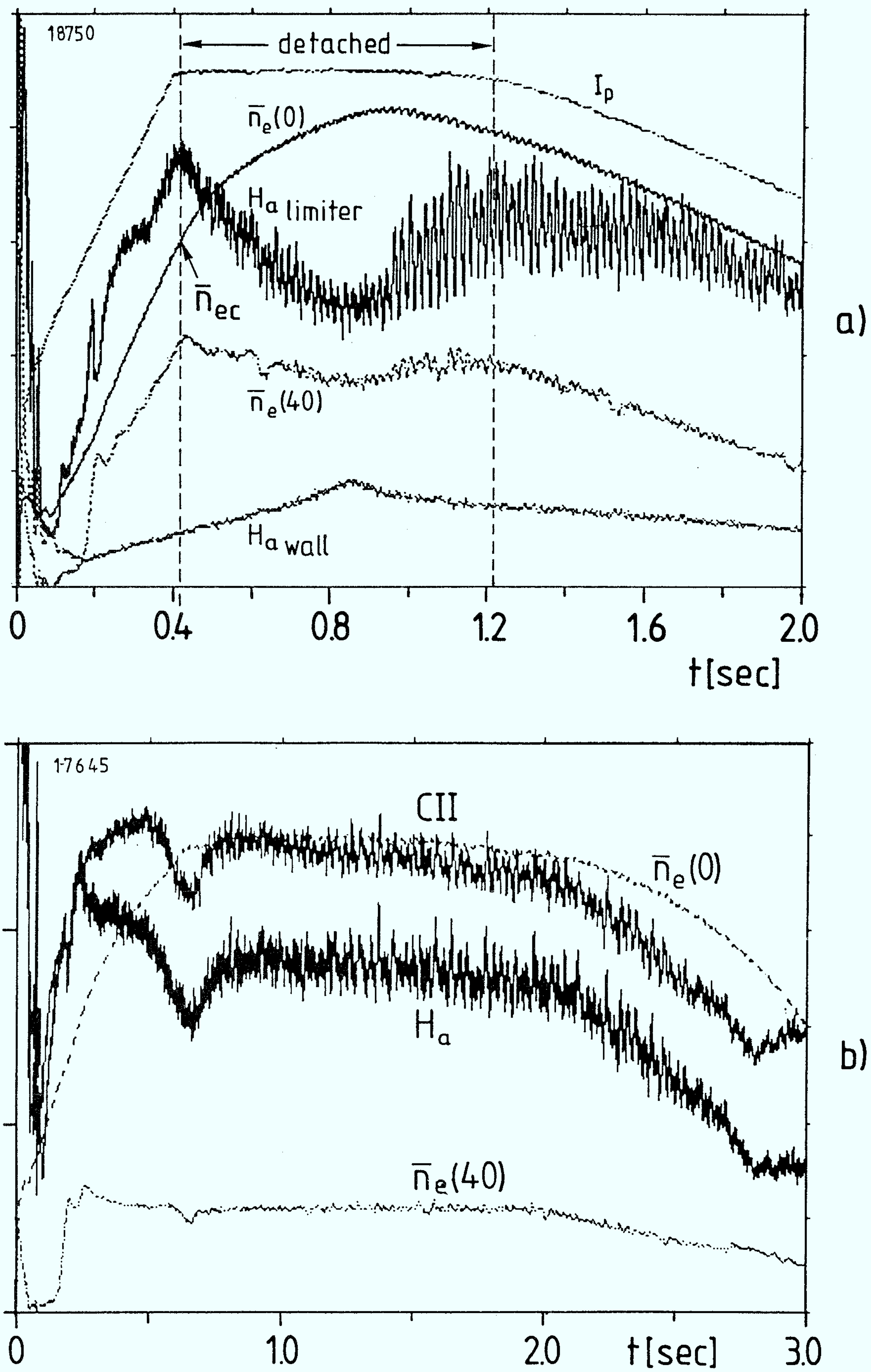

Fig. 2 Time traces of H_α(CII)-intensities at limiter and wall and of the line averaged electron-densities at r=0 cm and r=40 cm minor radius for a discharge a) being "detached" with peaking density and for a stationary discharge b) with "detachment" for the whole flat-top phase.

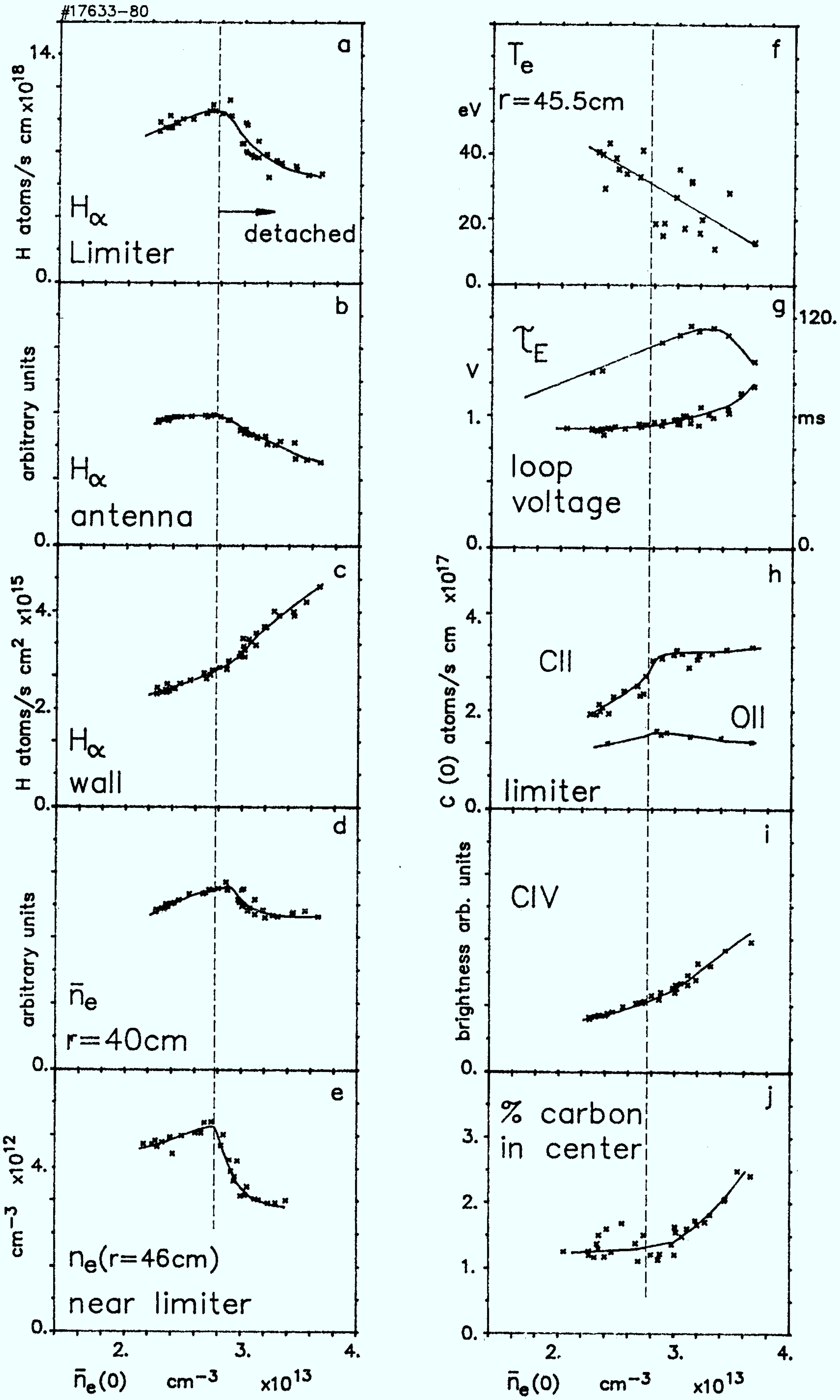

Fig. 3 Summary of signals obtained during the flat top phase of discharges from a density scan. The onset to "detachment" is at $\bar{n}_e = 2.8 \cdot 10^{13} cm^{-3}$. The diagnostics used are: a)-c) interference filters, d) HCN-interferometer, e) Li-oven, f) Thomson scattering, g) diamagnetic loop, h)-i) spectrometer, j) soft-x-rays.

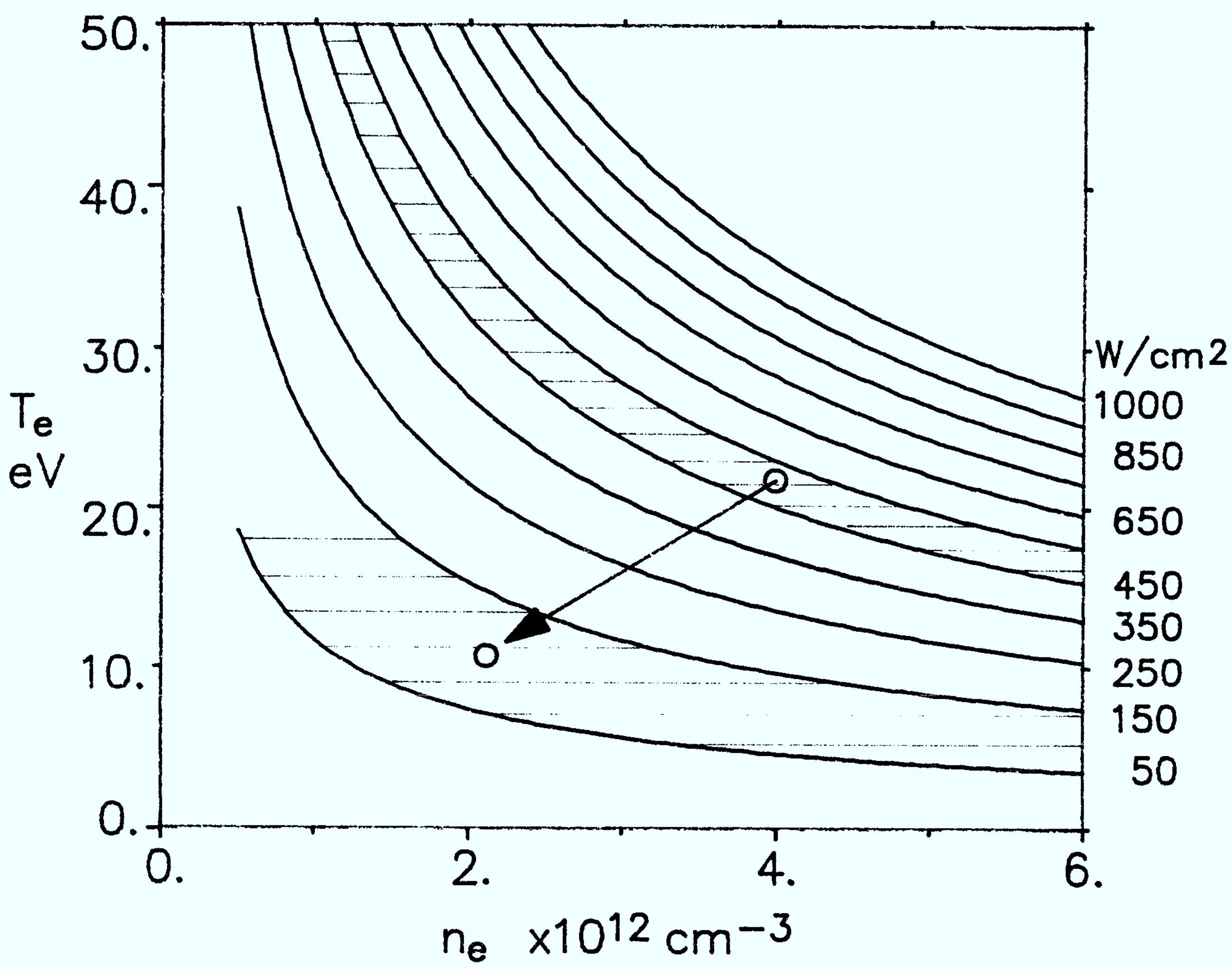

Fig. 4 Lines of constant heat flux onto the limiter surface depending on electron-density and -temperature at the edge calculated for deuterium. The arrow indicates a typical transition from "attached" to "detached" plasmas.

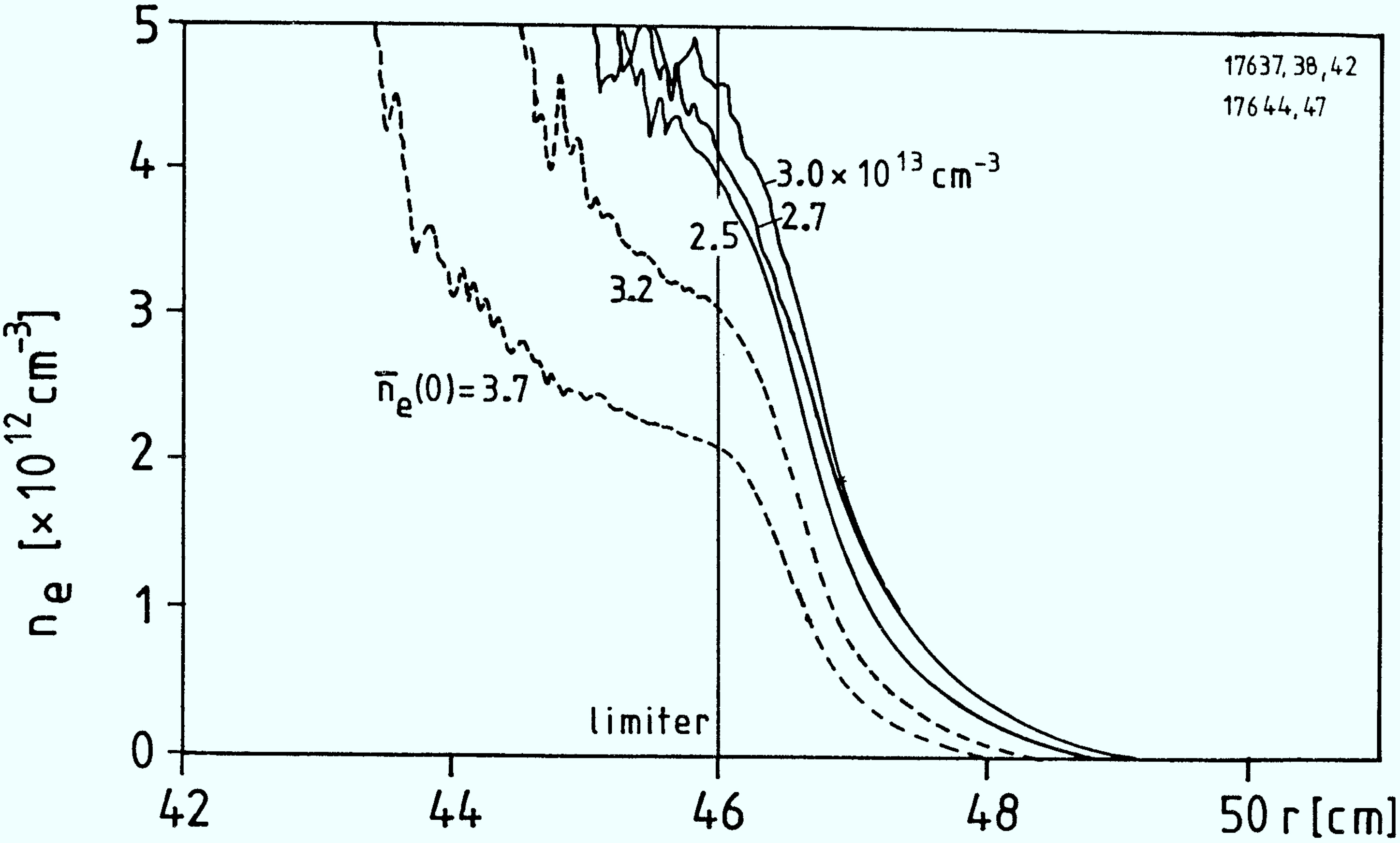

Fig. 5 Radial profiles of electron-density near the limiter measured with the use of the thermal Li-beam during the flat top phase of discharges with various central densities. The dashed lines correspond to "detached"-plasmas.

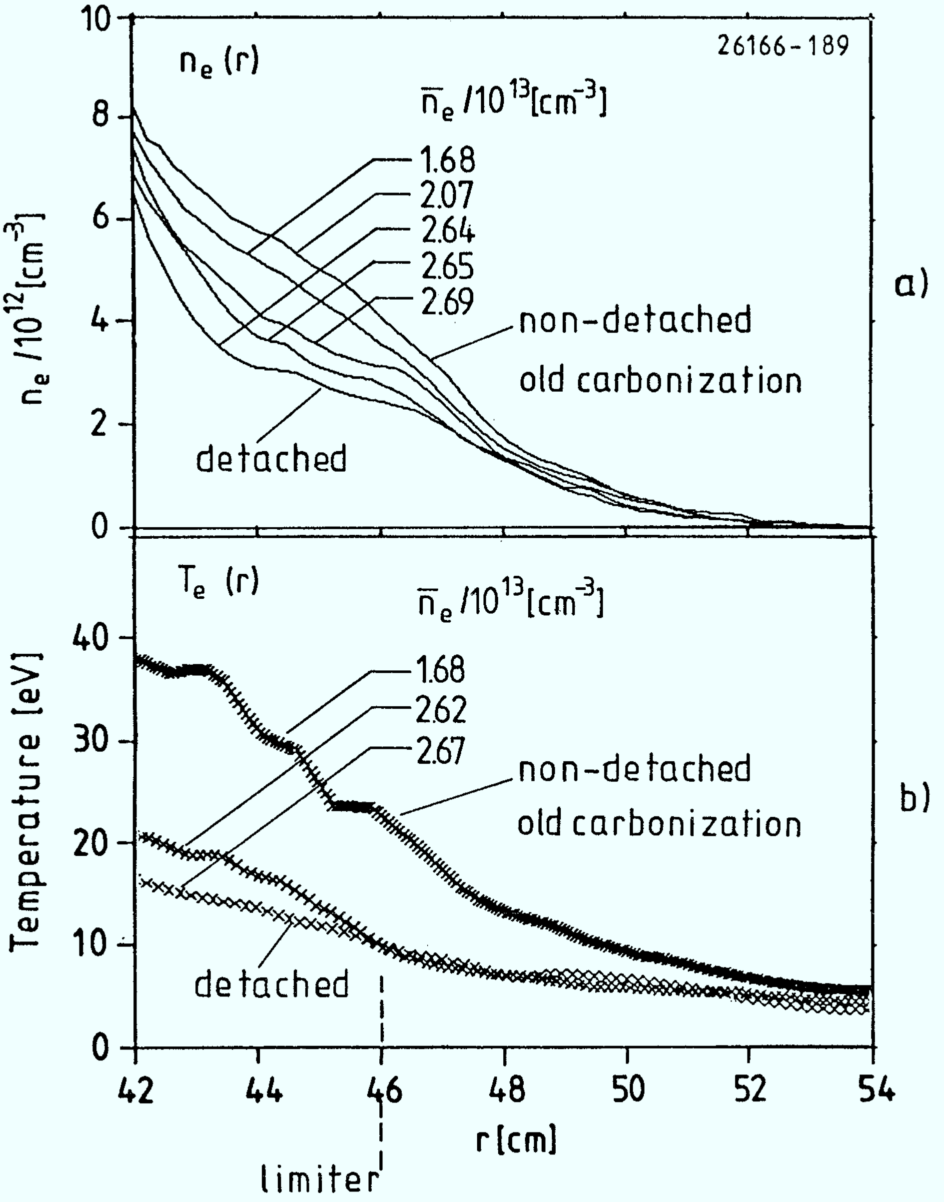

Fig. 6 n_e and T_e profiles measured with the use of 10 eV Li and C atom beams injected by laser ablation for discharges at different central densities.

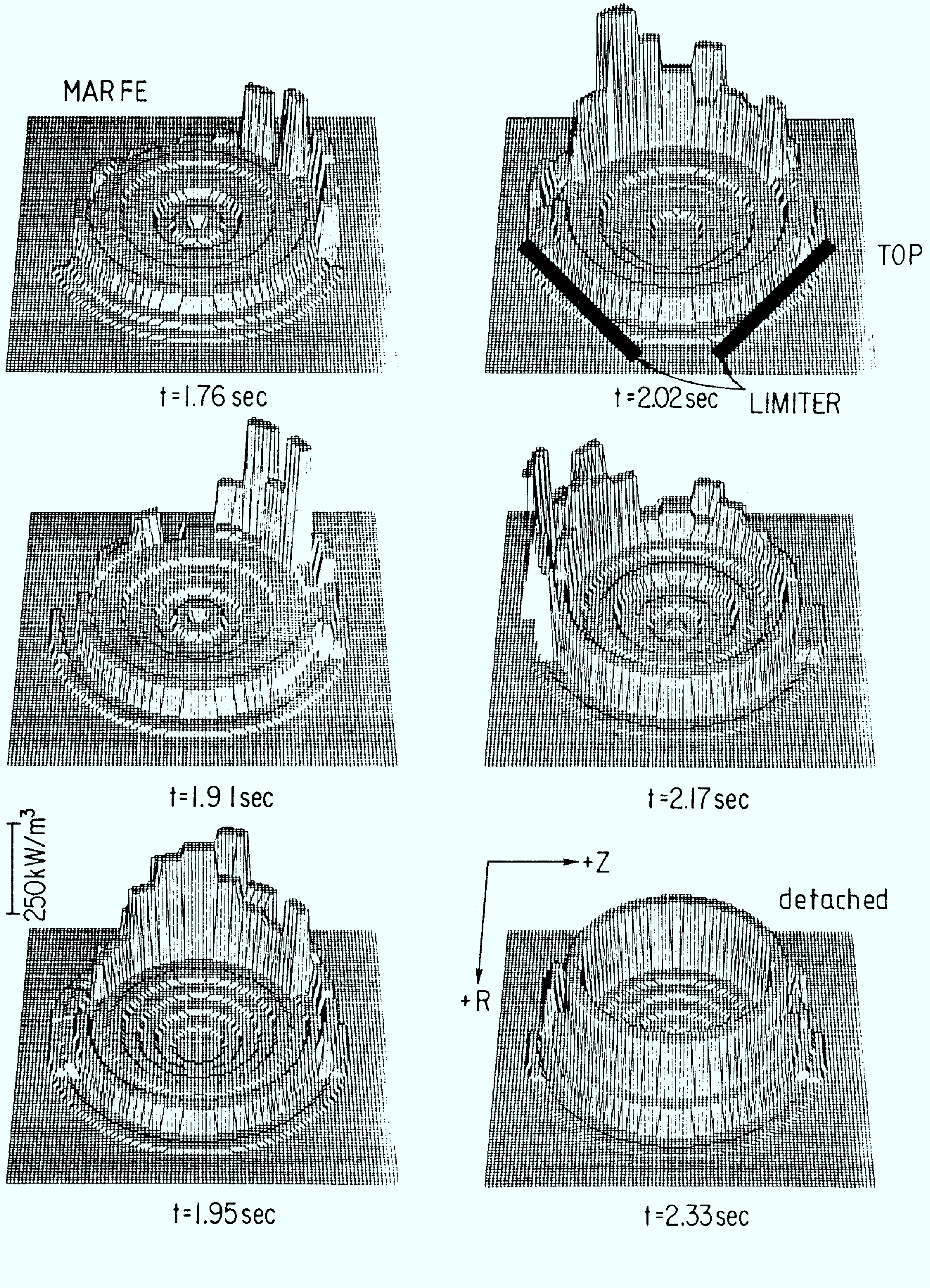

Fig. 7 Poloidal distribution of the radiated power in TFTR for the transition to a "detached"-plasma. [the fig. is taken from Boody, ref. 6]

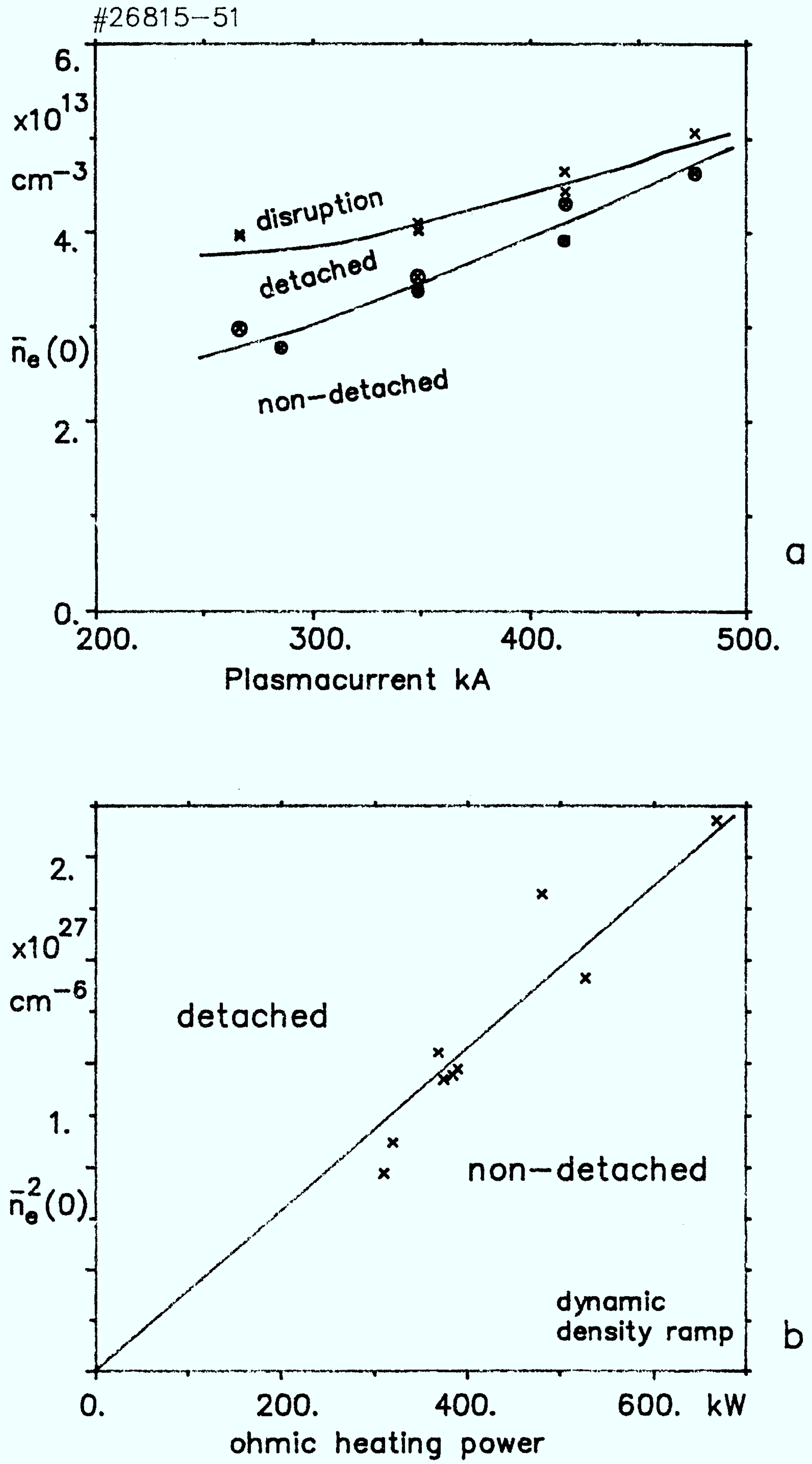

Fig. 8 a) Variation of the density for the onset of a "detached"-plasma $\bar{n}_{ec}$ and for the density limit with plasma current in discharges with a density ramp.
b) square of the critical density $\bar{n}_{ec}$ versus heating power.

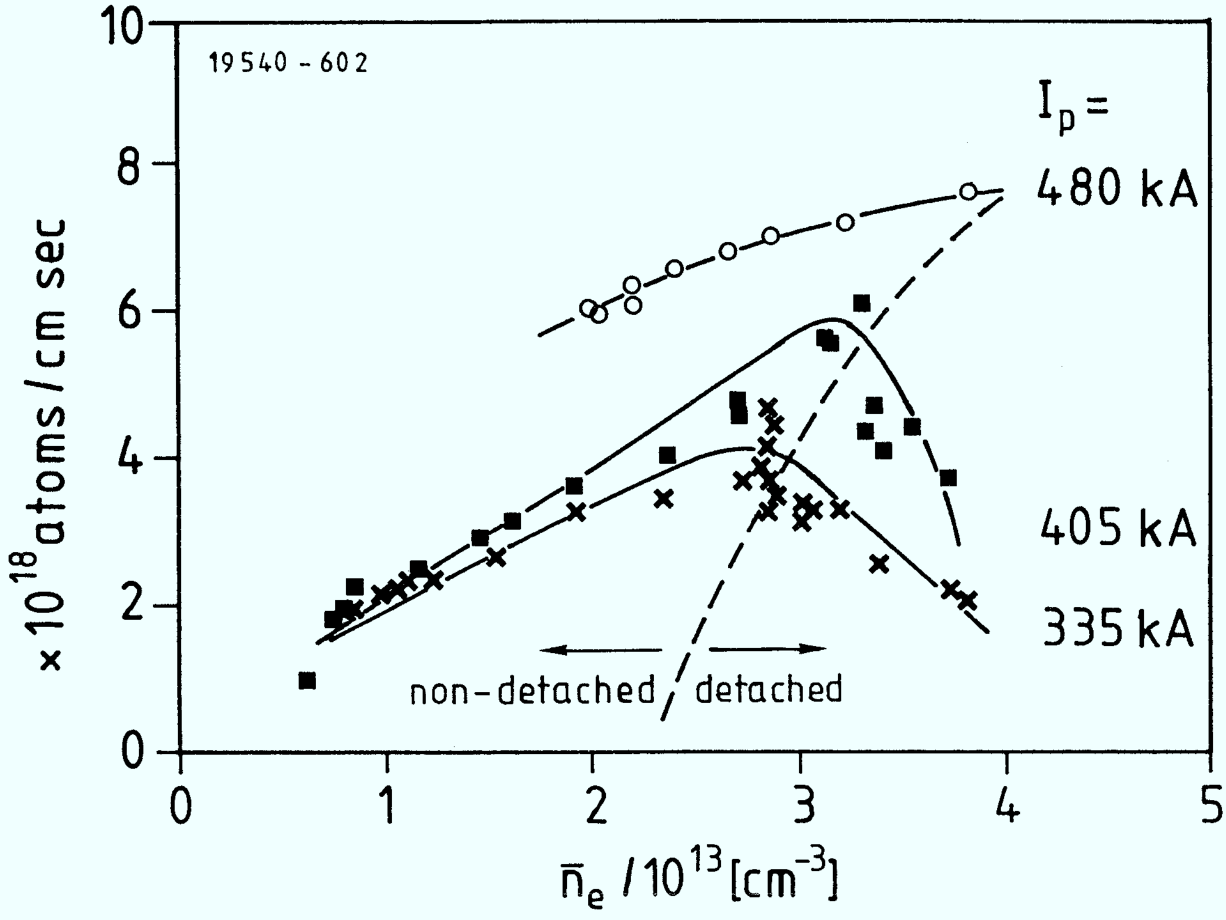

Fig. 9 Deuterium flux (D_α) as a function of central density for various plasma currents (flat top).

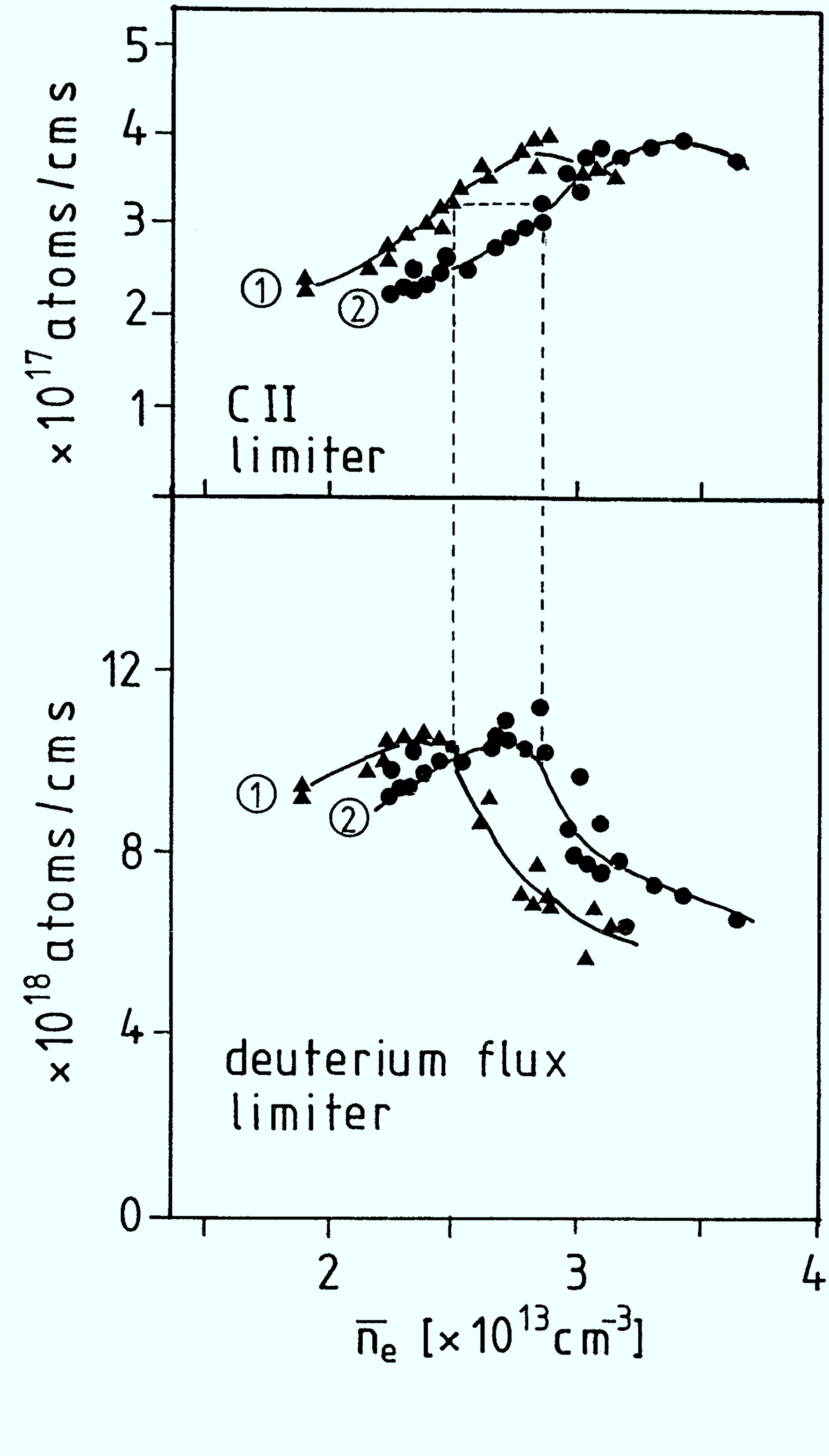

Fig. 10 Correlation of a) C-flux (CII) and b) D-flux (D_α) at the limiter for density scans at different impurity levels (conditioning). The dashed lines indicate the onset to a "detached"-plasma.

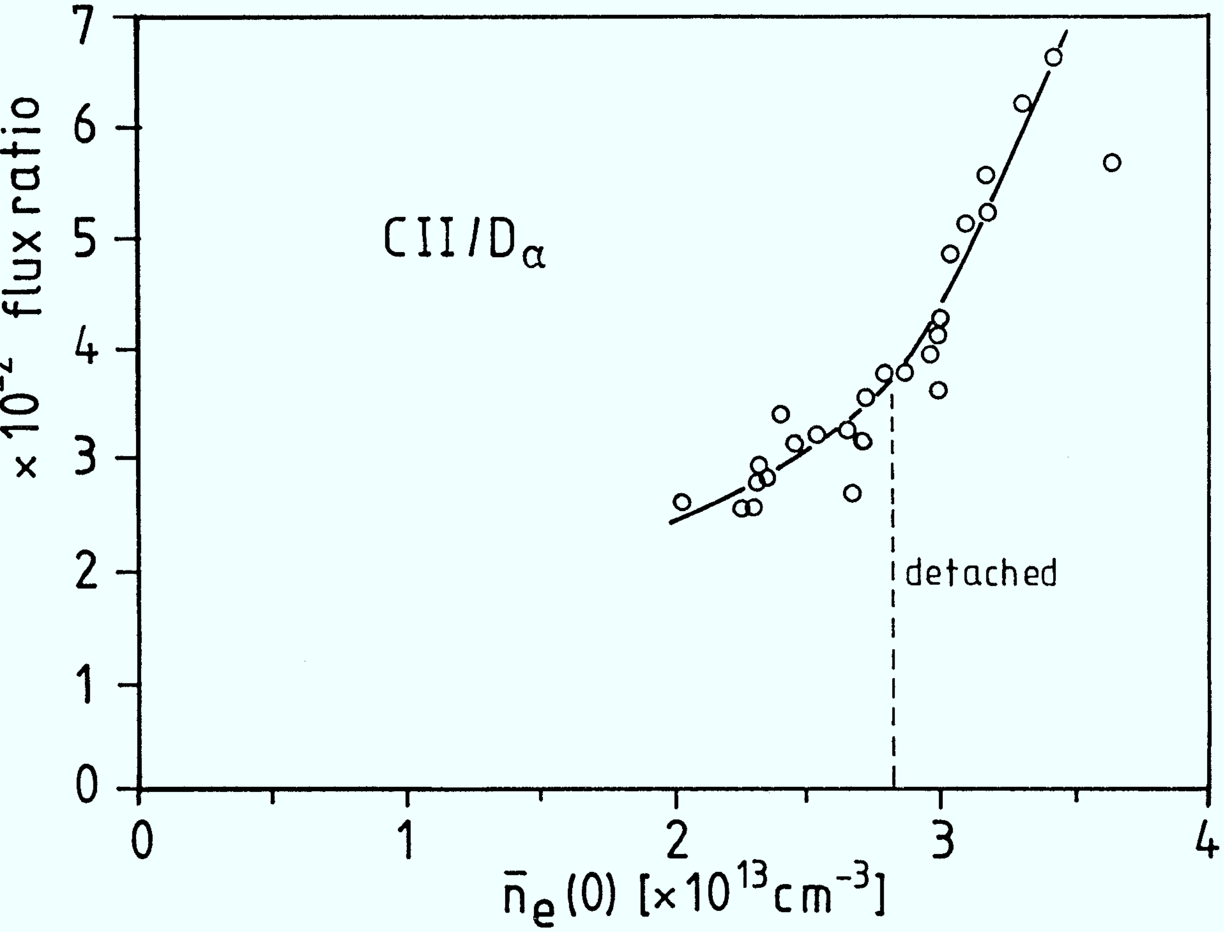

Fig. 11 Ratio of C- and D-fluxes at the limiter as a function of central electron-density.

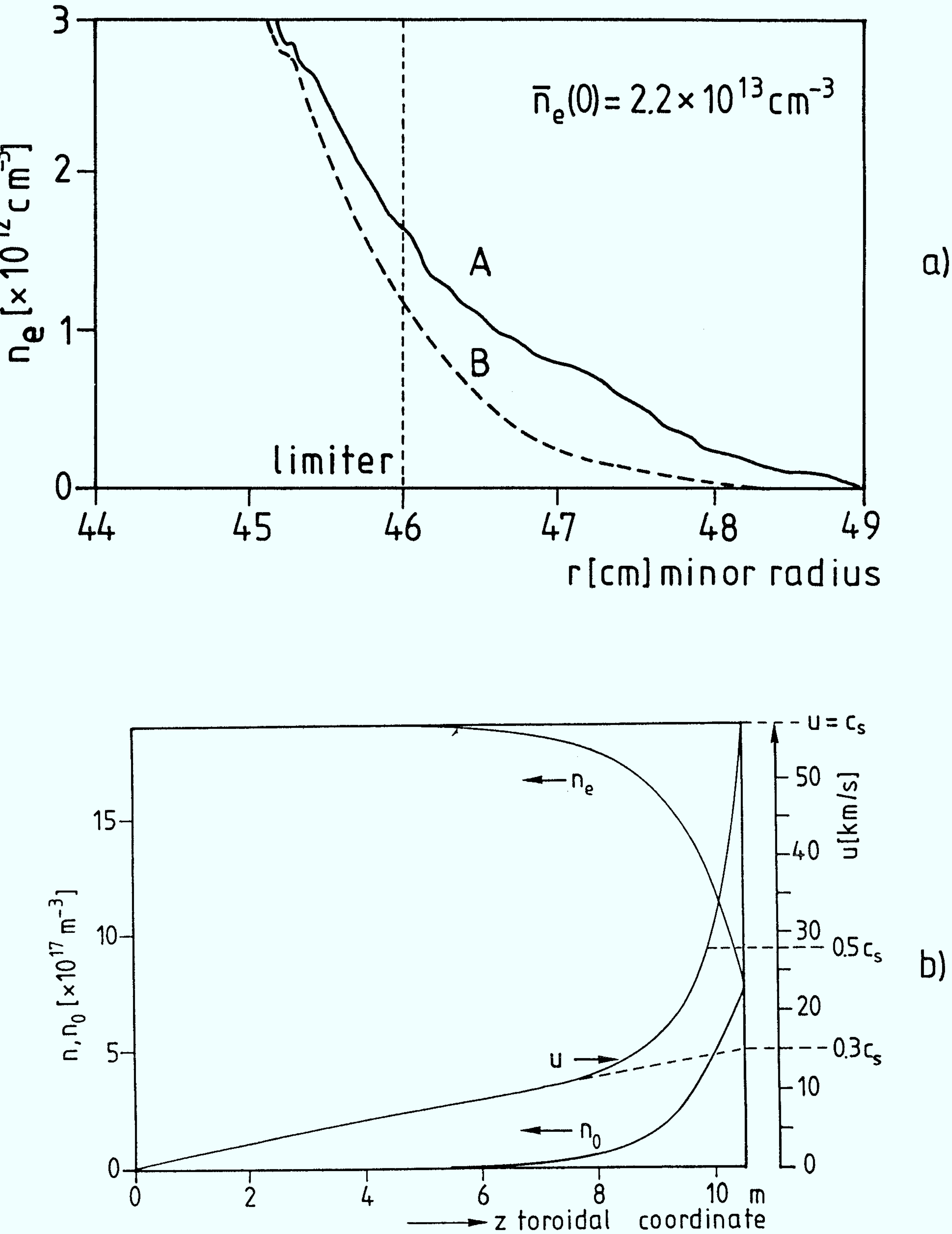

Fig. 12 a) Electron-density profiles at a toroidal location with short (B) and long (A) connection lengths with respect to the limiter (Li-oven diagnostics).
b) Calculated flow velocity u, density n_e and density of neutrals n_o along the plasma flow channel towards the limiter (2-d-model).

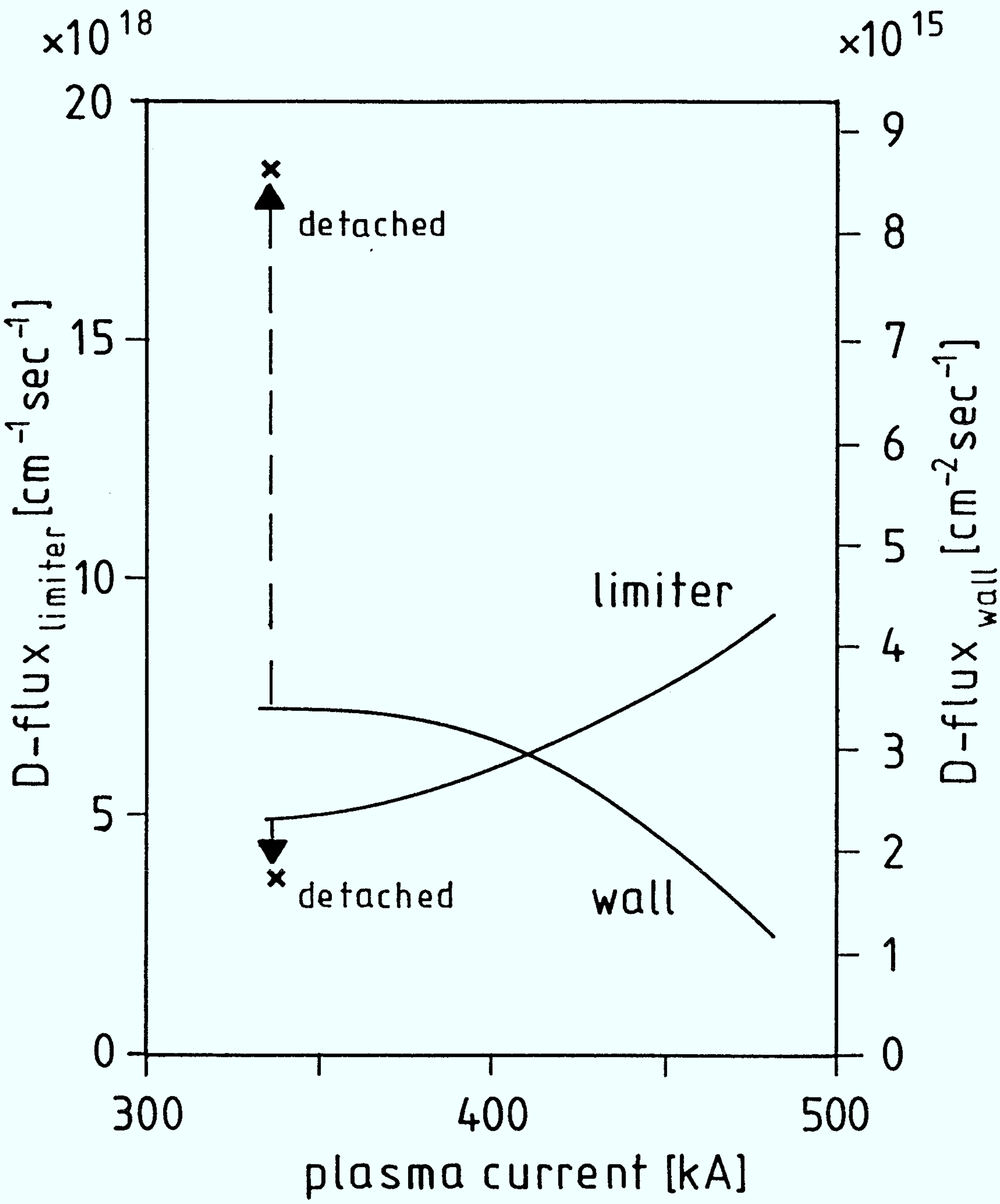

Fig. 13 D-fluxes at limiter and wall with constant central electron-density $\bar{n}_e=2.5\cdot10^{13}cm^{-3}$ and varying plasma current. For the "detached" case the density is $3.5\cdot10^{13}cm^{-3}$.

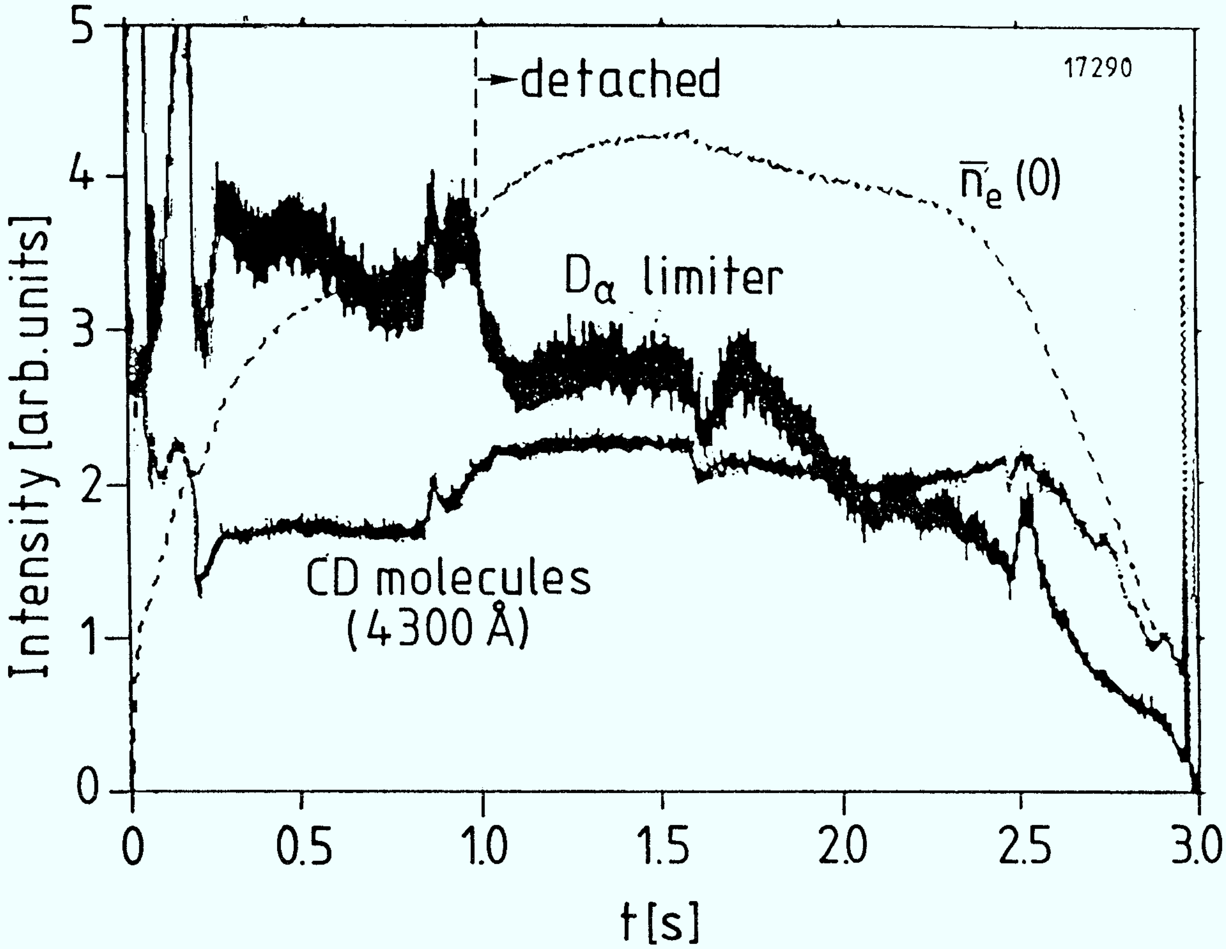

Fig. 14 Brightness of a molecular band emission (CD at 4300 Å, FWHM 20 Å) and D_α at the main limiter showing a transition to a "detached"-plasma induced by ICRF-heating.

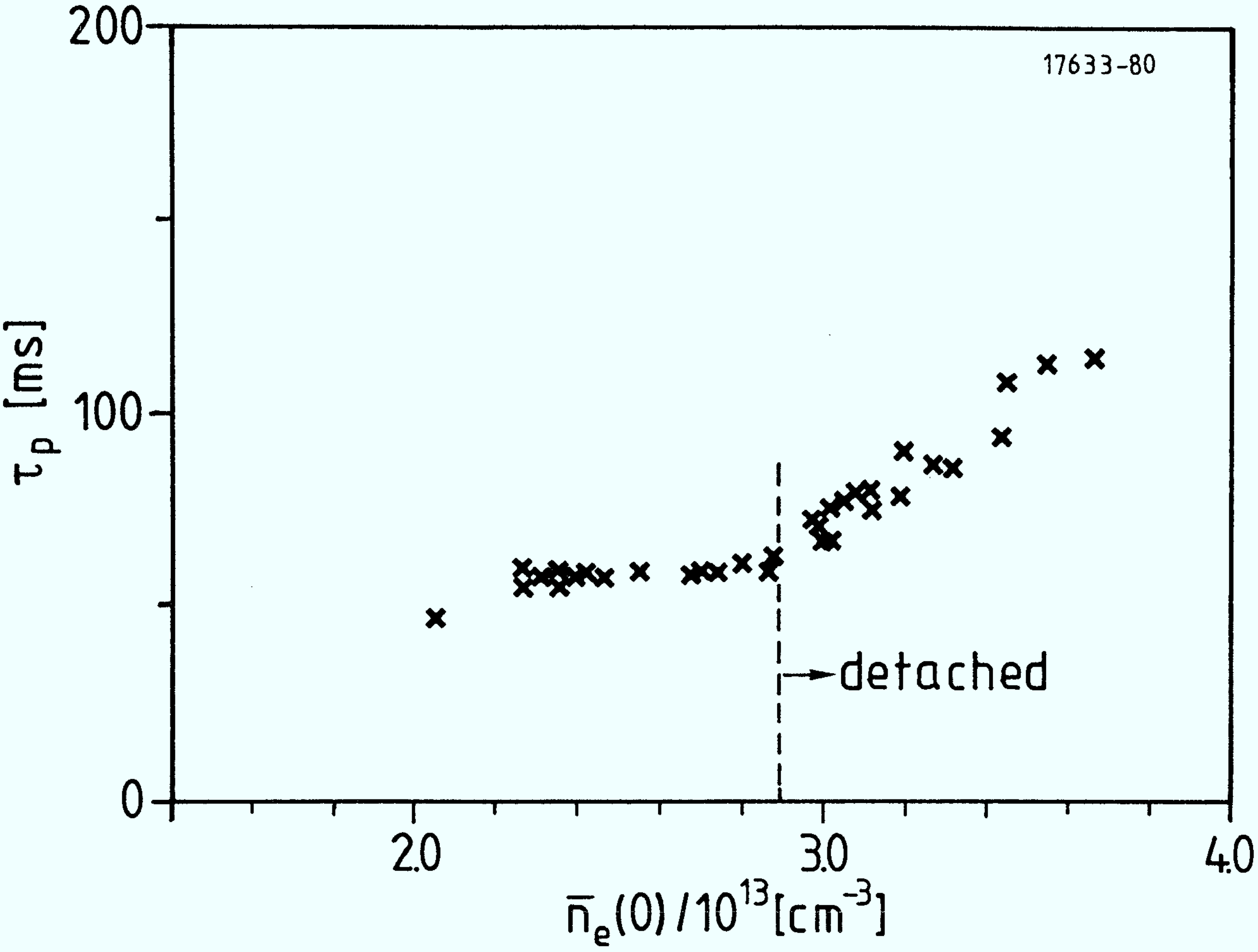

Fig. 15 Global particle confinement time τ_p as a function of central density (flat top), definition: $\tau_p = N_{tot} / [\, C_1 \int H_{\alpha limiter} + C_2 \int H_{\alpha wall} \,]$.

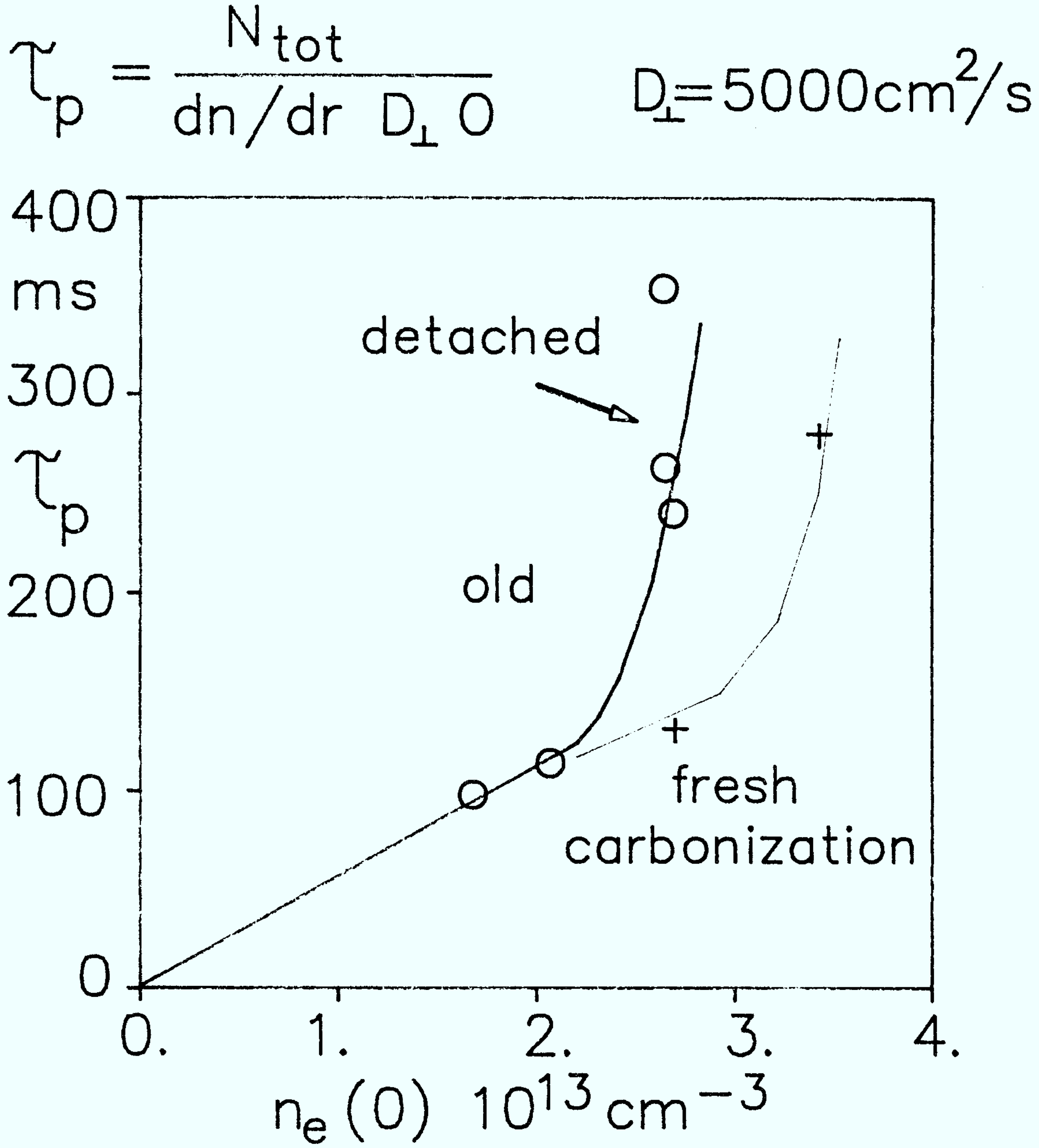

Fig. 16 Global particle confinement time τ_p as a function of central density (flat top). The particle flux is calculated from the measured density gradient at the edge of the scrape-off-layer assuming D=const.

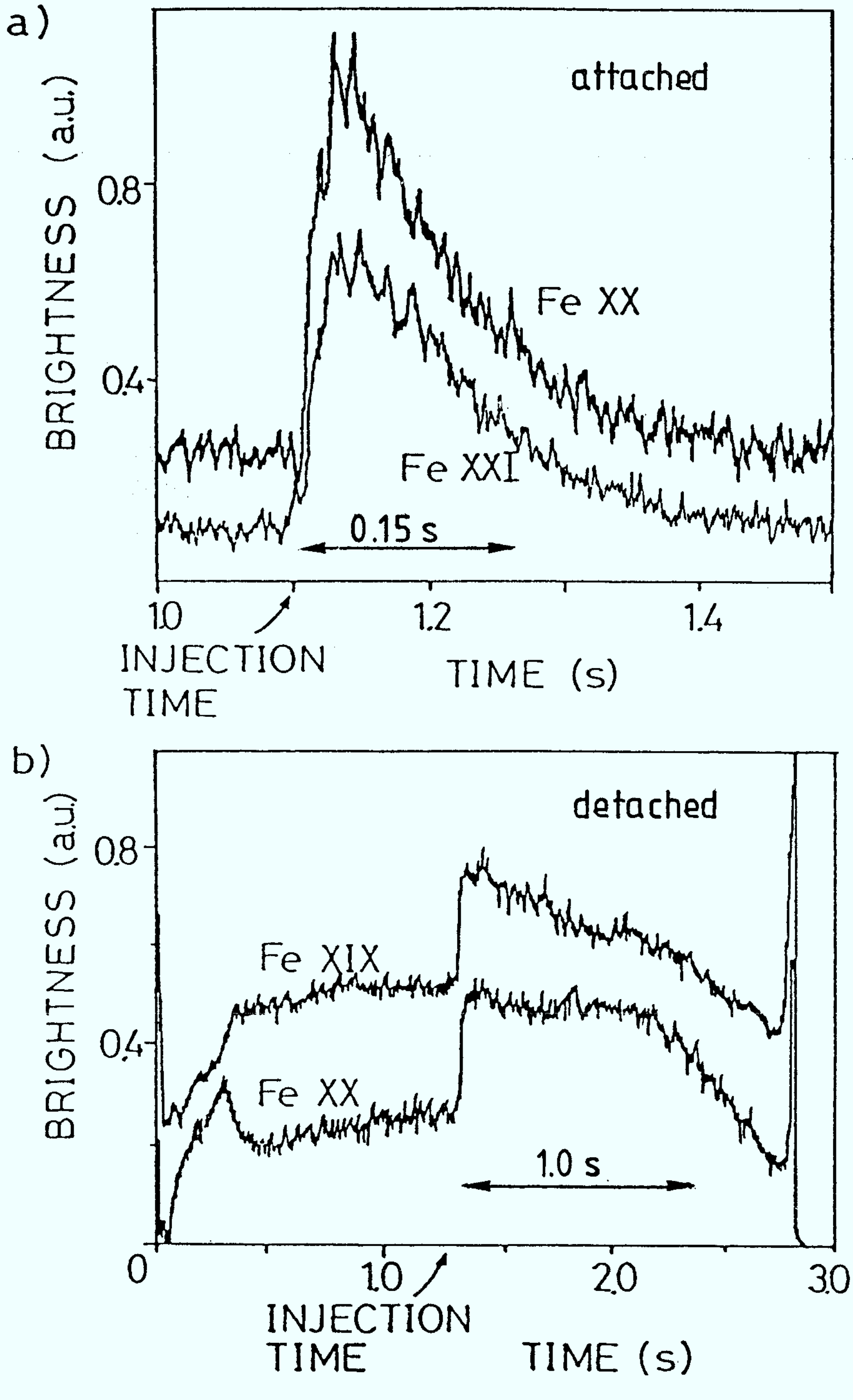

Fig. 17 Time traces of the radiation from highly ionized Fe after injection by laser ablation in two different discharges (attached and detached). [the figs. are taken from Castracane, ref.30]

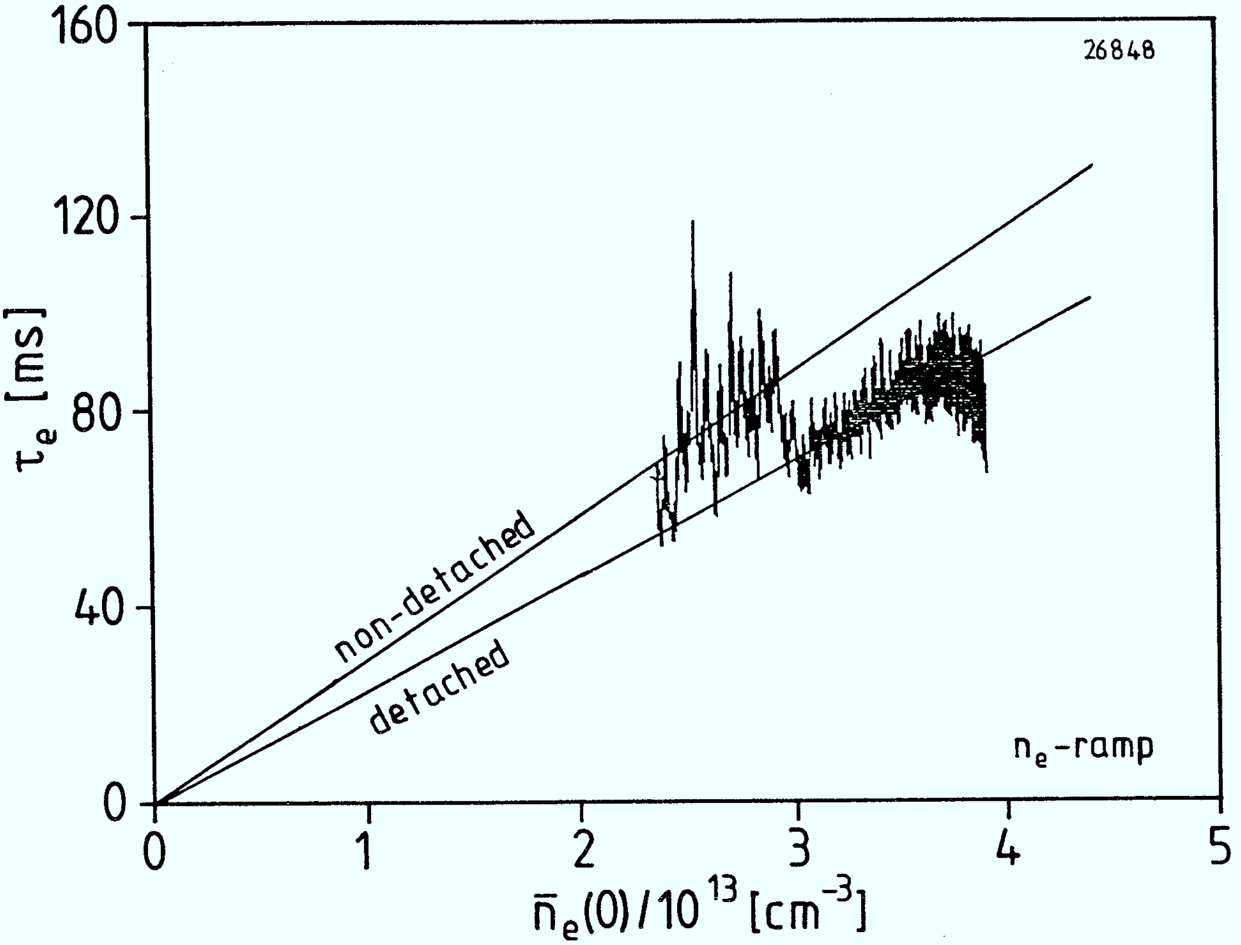

Fig. 18 Variation of the energy confinement time during a discharge with rising central electron-density and a transition to a "detached" state.

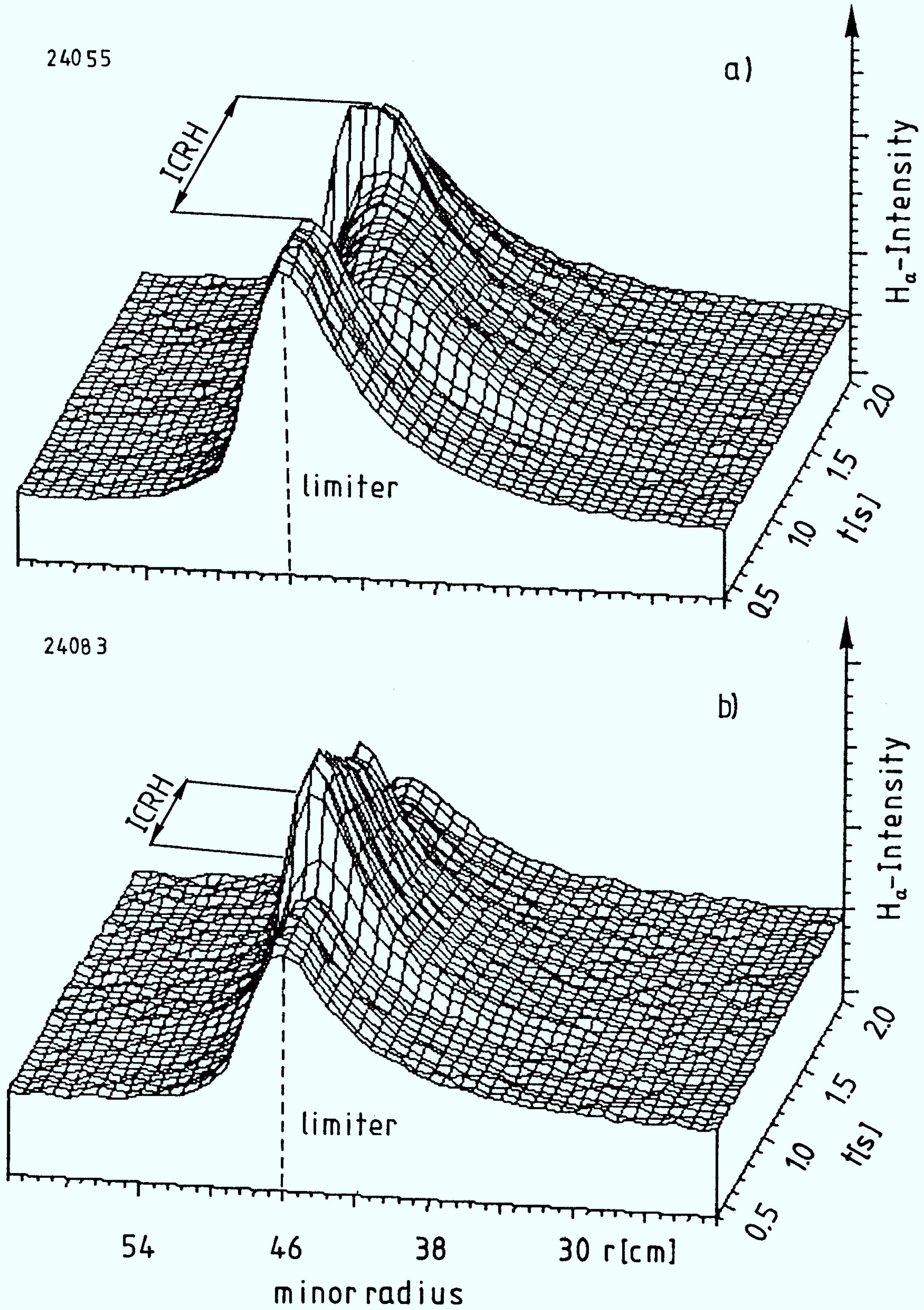

Fig. 19 Temporal H_α-intensity variation along the minor radius at the upper main limiter for two discharges with different impurity levels (20 min of RG-cleaning inbetween). The switch-on of ICRF-heating leads in case a) to a "detached"-plasma whereas in case b) the plasma remains "attached".

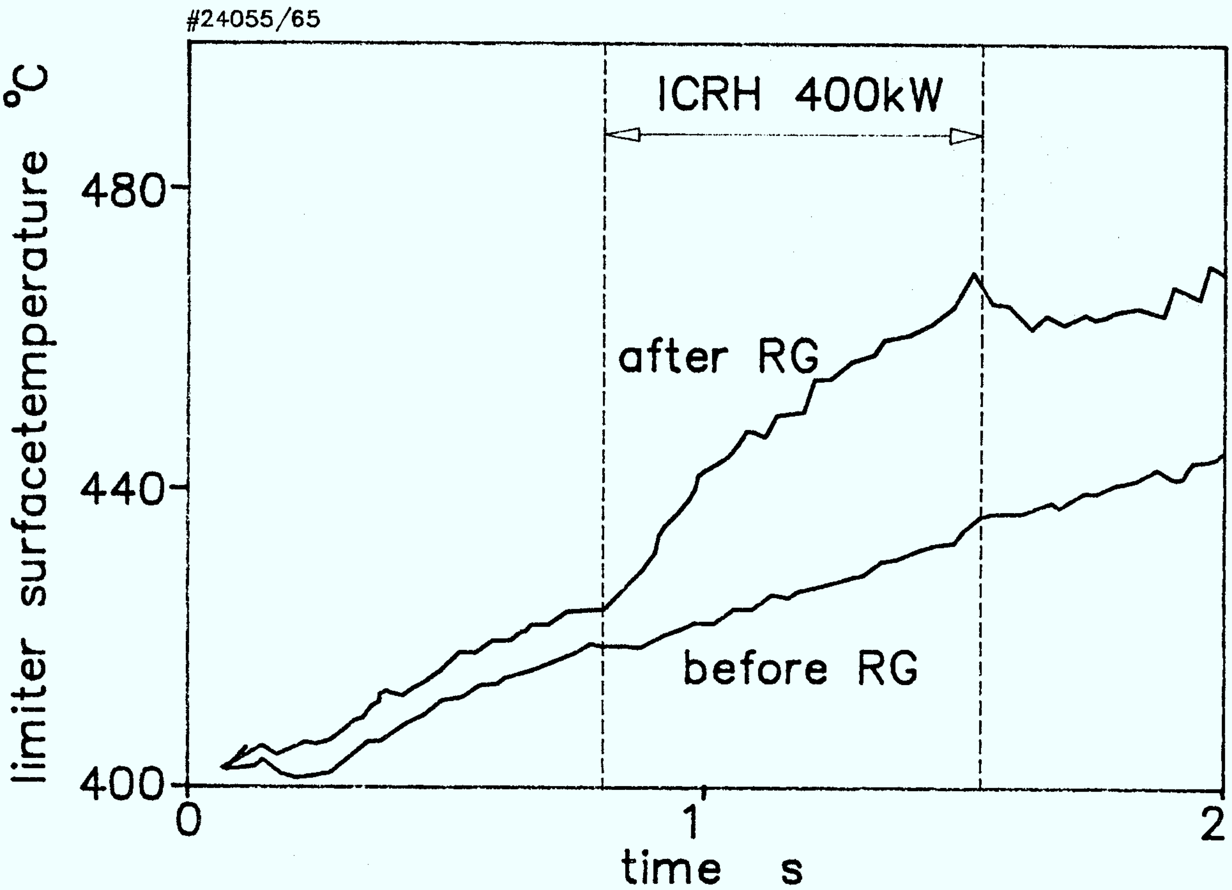

Fig. 20 Increase of the limiter surface temperature during discharges with ICRH. The plasma becomes "detached" with ICRH before the RG-cleaning procedure was applied.

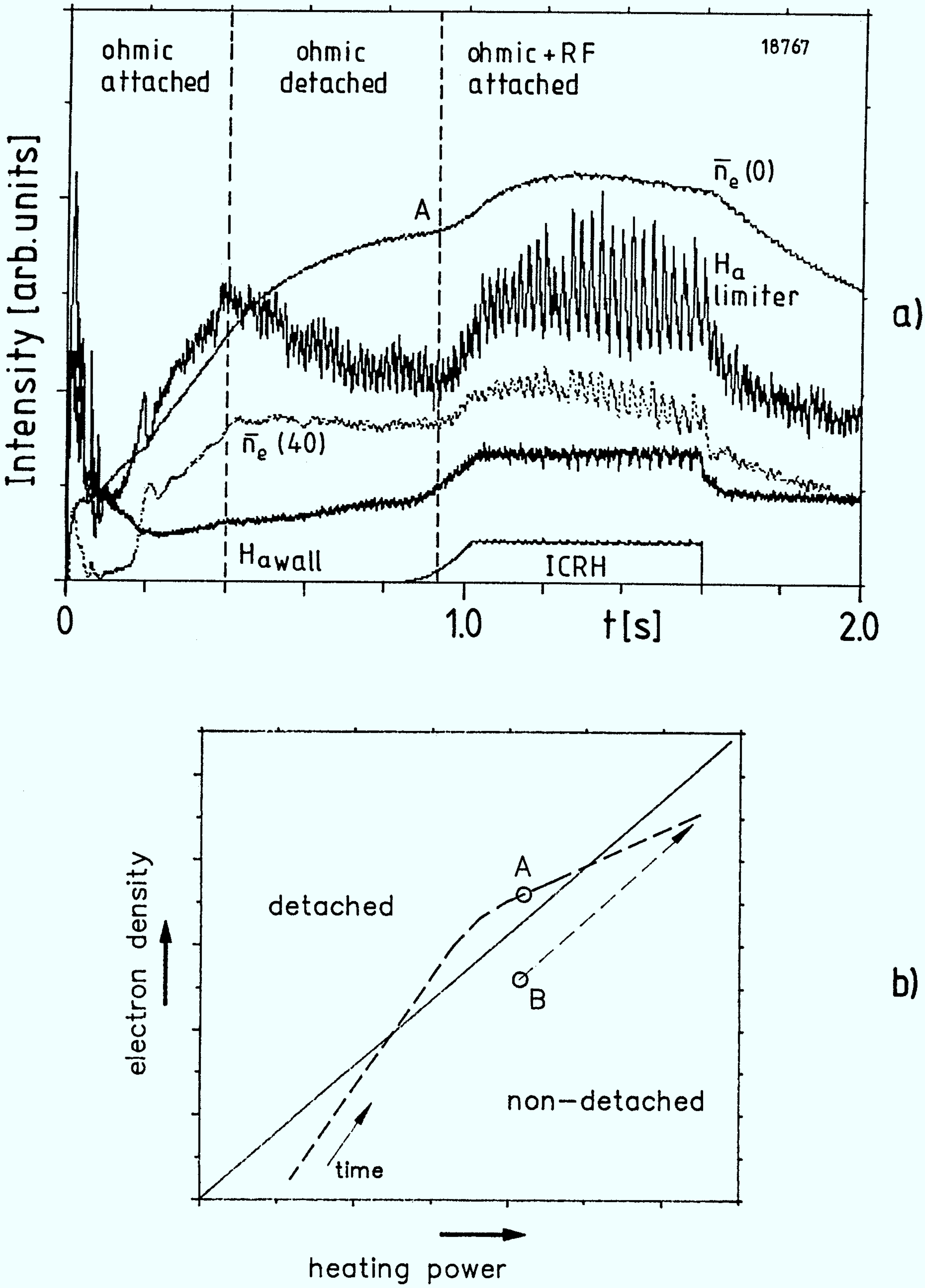

Fig. 21 a) Example for a "detached"-plasma being changed into "attached" conditions by the onset of ICRF-heating. b) Schematical display of the balance between the increase of $\bar{n}_e$ and P_{heat}, which determine the conditions for "detachment". The dashed line corresponds to the discharge in a).